Lipid bilayer stress-activated IRE-1 modulates autophagy during endoplasmic reticulum stress

Jhee Hong Koh*, Lei Wang*, Caroline Beaudoin-Chabot, Guillaume Thibault

School of Biological Sciences Nanyang Technological University, Singapore, 637551

*J.H.K. and L.W. contributed equally to this work.

Correspondence to:
Guillaume Thibault, Tel: +65 6592 1787; Fax: +65 6791 3856; email: thibault@ntu.edu.sg

Keywords: endoplasmic reticulum (ER), unfolded protein response (UPR), lipid bilayer stress, autophagy, metabolic disease

JCS Advance Online Article. Posted on 17 October 2018

SUMMARY STATEMENT

Lipid bilayer stress, genetically induced by membrane phospholipid imbalance, leads to the upregulation of autophagy through the ER stress-activated unfolded protein response, promoting cellular homeostasis.

ABSTRACT

Metabolic disorders such as nonalcoholic fatty liver disease (NAFLD) are emerging epidemics that affect the global population. One facet of these disorders is attributed to the disturbance of membrane lipid composition. Perturbation of endoplasmic reticulum (ER) homeostasis through alteration in membrane phospholipids activates the unfolded protein response (UPR) and causes dramatic transcriptional and translational changes in the cell. To restore cellular homeostasis, the three highly conserved UPR transducers ATF6, IRE1, and PERK mediate adaptive responses upon ER stress. The homeostatic UPR cascade is well characterised under conditions of proteotoxic stress, but much less so under lipid bilayer stress induced-UPR. Disrupted phosphatidylcholine (PC) synthesis in *C. elegans* causes lipid bilayer stress, lipid droplet accumulation and ER stress induction. Transcriptional profiling of PC-deficient worms shows a unique subset of genes regulated in a UPR-dependent manner that is independent from proteotoxic stress. Among these, we show that autophagy is modulated through the conserved IRE-1/XBP-1 axis, strongly suggesting of the importance of autophagy in maintaining cellular homeostasis during lipid bilayer induced-UPR.

INTRODUCTION

Lipid content within cells is tightly regulated to maintain cellular homeostasis and is crucial in many physiological processes including energy storage, signalling and membrane formation. The disruption in lipid homeostasis has been strongly associated with obesity and nonalcoholic fatty liver disease (NAFLD) (Puri et al., 2007, Tiniakos et al., 2010, Arendt et al., 2013, Doycheva et al., 2017), and is often characterised by excessive accumulation of lipids in liver, pancreatic and adipose tissues. Consequently, the inability of cells to alleviate such lipotoxic conditions results in a dysfunctional stress response and the induction of apoptosis that ultimate lead to a disease state (Hotamisligil and Erbay, 2008, Rinella and Sanyal, 2015). Altered hepatic phospholipids levels have been observed in murine models of nonalcoholic hepatosteatosis (NASH), a more aggressive form of NAFLD, which can develop into hepatic fibrosis and hepatocellular carcinoma (HCC) (Li et al., 2006, Fu et al., 2011b). Furthermore, the ratio of phosphatidylcholine (PC) to phosphatidylethanolamine (PE), the two major phospholipid species, has been associated with the survival and prognosis of liver function after partial hepatectomy in mice (Ling et al., 2012). As both PC and PE are the main lipids within the endoplasmic reticulum (ER) membrane, simultaneously blocking the two PC biosynthesis pathways by PE N-methyltransferase (PEMT) gene ablation and the lack of dietary choline leads to hepatic ER stress in mice, which correlates with steatosis progression (Li et al., 2005) (Fig. 1A). These observations link lipid bilayer stress, ER stress, and metabolic disease progression.

The ER is the hub of protein folding targeted to the secretory pathway (Schroder and Kaufman, 2005, Braakman and Bulleid, 2011). In addition to its role in protein homeostasis, the ER is the site of lipid metabolism that provides majority of the membrane lipids to the cell (Lagace and Ridgway, 2013, Wu et al., 2014). Long term disruption of lipid homeostasis triggers chronic ER stress, which is associated with metabolic diseases (Fu et al., 2011b, Han and Kaufman, 2016). To counter ER stress and maintain ER functionality, eukaryotes have evolved transcriptional and translational regulatory pathways collectively termed as the unfolded protein response (UPR) (Cox and Walter, 1996, Schroder and Kaufman, 2005, Shen et al., 2004). The highly conserved UPR programme exerts homeostatic control by sensing misfolded protein accumulation or membrane lipid bilayer stress at the ER (Walter and Ron, 2011, Volmer et al., 2013). As part of the programme, a subset of genes is upregulated to remodel various cellular pathways to ease stress and maintain viability, and the failure to reach ER homeostasis may result in cell death through apoptosis (Oyadomari et al., 2002, Wu et al., 2014, Mota et al., 2016).

In metazoa, the UPR consists of three conserved ER stress transmembrane transducers namely ATF6, IRE1 and PERK. Upon ER stress, each sensor activates their cognate downstream effectors resulting in general translational shutdown and the upregulation of target genes to restore cellular homeostasis (Walter and Ron, 2011, Wu et al., 2014). In the event of an acute response to excessive ER stress, the UPR programme leads to cell death through the IRE1 and PERK branches (Harding et al., 2003, Novoa et al., 2001). On the other hand, chronic ER stress triggers an adaptive response of the UPR programme that leads to differential expression of pro-survival signals and stabilisation of the UPR machinery, thereby bypassing apoptosis induction (Rutkowski et al., 2006, Rubio et al., 2011, Kim et al., 2017).

Previously, we have demonstrated that changes in membrane lipid composition through the ablation of the *de novo* PC biosynthesis gene *OPI3* (*PEMT* orthologue) activate the essential intervention of the UPR to remodel the protein homeostasis network in budding yeast (Thibault et al., 2012, Ng et al., 2017). The UPR is directly activated from ER membrane lipid bilayer stress independent from the accumulation of misfolded proteins (Promlek et al., 2011, Volmer et al., 2013, Ho et al., 2018, Tam et al., 2018). Similar to the NAFLD mouse model lacking the *PEMT* gene (Li et al., 2006, Li et al., 2005) and our yeast model deleted for the *OPI3* gene (Thibault et al., 2012, Ng et al., 2017), *C. elegans* models have been developed to block PC synthesis by the loss-of-function *(lof)* mutants of *PEMT* orthologues *pmt-1* and *pmt-2* or the upstream precursor S-adenosylmethionine synthetase *sams-1* (Brendza et al., 2007, Li et al., 2011, Walker et al., 2011, Ding et al., 2015) (Fig. 1A).

Excessive proteins accumulation during proteotoxicity-induced ER stress has been shown to activate autophagy as the accumulation of misfolded proteins exceeds the capacity of the ER-associated degradation for their clearance (Kouroku et al., 2007, Senft and Ronai, 2015), but little is known on its role during lipid bilayer stress-induced UPR. In this study, we characterised the UPR function during chronic lipid bilayer stress-induced ER stress. We proposed that lipid bilayer stress may elicit chronic ER stress response that is distinct from that resulting from acute ER stress. In *C. elegans*, we silenced *pmt-2* to attenuate PC synthesis in the UPR mutant animals; *atf-6(lof)*, *ire-1(lof)* and *pek-1(lof)*. As expected, genetic ablation of *pmt-2* resulted in the perturbation of lipid homeostasis with significantly decreased PC levels, which then correlated with UPR activation. Although conventionally seen as a linear response to ER stress, our findings demonstrate a strikingly different outcome of the UPR programme when activated by lipid bilayer stress (UPR^{LBS}) as opposed to proteotoxic stress (UPR^{PT}). More importantly, we reveal that autophagy is modulated by the IRE-1/XBP-1 axis upon lipid bilayer stress-induced UPR, suggesting the importance of autophagy to maintain cellular homeostasis during lipid bilayer stress.

RESULTS

The attenuation of *pmt-2* activates the UPR by reducing total phosphatidylcholine

PMT-1 and *PMT-2* are both required for the synthesis of PC from PE in *C. elegans* (Palavalli et al., 2006, Brendza et al., 2007, Li et al., 2011) (Fig. 1A). In the absence of dietary choline, both genes are essential for the development of *C. elegans,* and silencing either genes from stage-one (L1) larvae leads to sterility (Brendza et al., 2007). PC cannot be obtained from standard laboratory worm diet as the conventionally used *E. coli* strains OP50 and HT115(DE3) lack PC (Morein et al., 1996, Oursel et al., 2007). Thus, PC levels in worms can be altered by genetically manipulating *pmt-1* or *pmt-2* to induce lipid bilayer stress (LBS) thereby activating the UPR (Fig. S1C). To better understand the role of the UPR during LBS, we subjected synchronised L1 worms to *pmt-2* RNA interference (RNAi) for 48 h. Two-day RNAi feeding was sufficient to decrease *pmt-2* mRNA in wild-type (WT) animals close to the background signal of *pmt-2(lof)* (Fig. 1B). As previously reported, *pmt-2*(RNAi) animals showed a developmental defect characterised by reduced body size, which is rescued by choline supplementation

(Fig. S1A,B) (Palavalli et al., 2006). PC is synthesised from choline through the Kennedy pathway (Fig. 1A). Supplementing *pmt-2(RNAi)* animals with 30 mM choline was sufficient to prevent UPR activation while the growth defect was alleviated with 60 mM choline (Fig. S1A-C). To further characterise *pmt-2(RNAi)* worms, PC was separated from the total lipid extract of worms by thin layer chromatography (TLC). This was followed by a transesterification reaction to derive fatty acid methyl esters (FAMEs) specifically from PC, which were further quantified by gas chromatography with flame ionisation detector (GC-FID). We found that the PC level in *pmt-2(RNAi)* worms was markedly reduced to 36% of the vector control worms (Fig. 1C). Attenuating *pmt-2* expression was not sufficient to fully eliminate PC in WT animals due to the large phospholipid reserve of stage L1 worms in addition to the long half-lives of phospholipids (Dowd et al., 2001). As LBS can lead to ER stress, we measured the transcriptional levels of the UPR-induced ER-resident molecular chaperone Hsp70 family (Urano et al., 2002). The mRNA levels for both human Hsp70 orthologues, *hsp-3* and *hsp-4*, were upregulated transcriptionally in *pmt-2(RNAi)* worms compared to WT (Fig. 1D). The mRNA level of *hsp-3* in *pmt-2(RNAi)* worms was similar to that of WT worms incubated with the strong UPR inducer tunicamycin (Tm) for 4 h. Tm inhibits protein *N*-glycosylation leading to a severe accumulation of unfolded proteins in the ER (Ericson et al., 1977). In contrast, *hsp-4* mRNA level was remarkably higher in Tm-treated animals compared to LBS. This result suggests that *hsp-4* expression might be modulated differently by the UPR programme depending on the nature of stress. As the UPR is activated from low PC, *C. elegans* subjected to *pmt-2* RNAi mimics NAFLD where altered PC/PE ratios and UPR activation are interconnected (Ozcan et al., 2004, Fu et al., 2011a, Thibault et al., 2012, Ng et al., 2017).

Attenuated phosphatidylcholine synthesis leads to lipid droplet accumulation

To investigate the regulatory role of the three ER stress transducers during LBS (Shen et al., 2005), *atf-6(lof), ire-1(lof)* and *pek-1(lof)* mutant worms were subjected to *pmt-2* RNAi as described above (Fig. S2A). The simultaneous ablation of two or three UPR branches is not possible as any combination is lethal (Shen et al., 2005). Treatment with *pmt-2* RNAi resulted in the reduction of PC across the three UPR mutants that is comparable to WT worms (Figs 2A, S2B). The UPR transducers regulate lipid metabolism where XBP-1 downstream of IRE-1 is responsible for phospholipid synthesis (Sriburi et al., 2004). Hence, it is unsurprising that *ire-1(lof)* worms have decreased PC compared to WT in its untreated condition (Fig. 2A). To quantify fatty acids (FAs) composition of PC and its precursor PE during lipid bilayer stress, both phospholipids were separated from total lipid extracts by TLC and quantified by GC-FID as described earlier. As expected, PC depletion in the UPR mutants and WT worms caused a significant reduction of all FAs derived from PC except for margaric acid (C17:0), α-linolenic acid (C18:3n3) and eicosadienoic acid (C20:2), indicating a general disturbance in the PC metabolic pathways during lipid bilayer stress (Fig. 2B). However, levels of FAs derived from PE were largely unmodified across the strains as *pmt-2* RNAi leads to the accumulation of the downstream phospholipid intermediate monomethyl-phosphatidylethanolamine (MMPE) (Fig. 1A). As a reduction in PC level leads to lipid droplet (LD) accumulation in eukaryotes (Li et al., 2011, Walker et al., 2011, Thibault et al., 2012, Horl et al., 2011), Sudan Black staining of fixed worms treated with *pmt-2* RNAi was carried out to visualise lipid droplets by Nomarski microscopy (Figs 2C, S3A). To compare LD

expansion in *pmt-2* RNAi treated worms, the diameter of LDs was measured and classified into small (0.8 - 3 µM), medium (3.1 - 6 µM) and large (> 6 µM) groups. We observed accumulation of large LDs but fewer total LDs in WT, *atf-6(lof)*, *ire-1(lof)*, and *pek-1(lof)* worms treated with *pmt-2* RNAi, corresponding to previous study in *sams-1(lof)* worms where PC is also reduced (Ding et al., 2015).

To ensure that *pmt-2* RNAi treatment is sufficient to induce ER stress in the UPR mutants, we monitored the mRNA expression of two downstream target genes of IRE-1, *hsp-3* and *hsp-4*, by quantitative RT-PCR. As expected, both ER-resident chaperones *hsp-3* and *hsp-4* levels were significantly increased upon *pmt-2* RNAi and tunicamycin treatments in WT and mutant strains with the exception of *ire-1(lof)* (Fig. 2D,E). Activation of the UPR from LBS was further validated *in vivo* by immunoblotting using the *phsp-4::gfp* reporter animal (Calfon et al., 2002). Consistent with *hsp-4* mRNA levels, *pmt-2* RNAi treatment resulted in almost two-fold increase in GFP in *phsp-4::gfp* animals while tunicamycin induced stronger upregulation (Fig. 2F). As expected, an increase in GFP was not detected in *xbp-1;phsp-4::gfp* animals treated with *pmt-2* RNAi nor with tunicamycin as HSP-4 is specifically upregulated from the IRE-1/XBP-1 axis upon ER stress (Acosta-Alvear et al., 2007).

UPR^{LBS} upregulates a distinct subset of genes from UPR^{PT}

Several studies suggest that the essential role of the UPR in maintaining metabolic and lipid homeostasis is highly conserved across species [for reviews, see (Volmer and Ron, 2015, Han and Kaufman, 2016)]. A novel ER stress sensing mechanism was proposed in which the UPR is activated by lipid bilayer stress independently of unfolded protein accumulation in the ER (Promlek et al., 2011, Volmer et al., 2013, Halbleib et al., 2017). Thus, ER stress triggered by proteotoxic stress or lipid bilayer stress might differentially modulate the UPR to reach cellular homeostasis. To answer this question, DNA microarray analysis was performed using RNA extracted from WT, *atf-6(lof)*, *ire-1(lof)* and *pek-1(lof)* animals treated with *pmt-2* RNAi. WT worms incubated with tunicamycin for 4 h were included in the analysis to identify genes modulated by proteotoxic-induced UPR (UPR^{PT}) and subsequently uncouple those specifically modulated by lipid bilayer stress-induced UPR (UPR^{LBS}). To validate the quality of microarray data, qPCR was performed on a subset of genes (Fig. S4A,C). Overall, 2603 and 1745 genes were upregulated and downregulated, respectively, in *pmt-2(RNAi)* animals compared to WT (Fig. 3A, Table S2, GEO: GSE99763). In addition, tunicamycin-treated WT worms showed upregulation of 1258 genes and downregulation of 1473 others. Only 492 and 420 genes were similarly upregulated and downregulated, respectively, from both UPR^{LBS} and UPR^{PT}, thereby suggesting these groups of genes are commonly modulated from the UPR regardless of the source of ER stress.

To explore how the UPR elicits a differential stress response during lipid bilayer stress and proteotoxic stress, we filtered the 2111 gene candidates that were upregulated only in *pmt-2(RNAi)* animals and excluding genes upregulated in tunicamycin-treated animals, respectively. Genes with unaltered expression in at least one of the UPR mutants subjected to *pmt-2* RNAi are considered to be modulated by UPR^{LBS}. From these criteria, 1069 genes were upregulated in a UPR^{LBS}-dependent manner (Fig. 3B, Table S3). We identified 181, 417, and 25 genes that are specifically upregulated from ATF-6, IRE-1,

and PEK-1 branches, respectively, while 446 genes are modulated from at least two of the three UPR branches, suggesting compensatory roles of one or more UPR transducers in the absence of the other branches. In addition, we grouped genes with at least 1.5-fold change by hierarchical clustering (Fig. 3C, Table S4). This allowed us to visualise genes that were similarly regulated throughout the array from UPR^{LBS}. Manual inspection of our array data demonstrates that the upregulation of known UPR target genes are in agreement with previous reports (Fig. 3D) (Travers et al., 2000, Shen et al., 2005, Thibault et al., 2011).

To further understand the role of the UPR^{LBS} programme, we performed functional annotation for the 1069, 181, 417, and 25 upregulated genes identified from *pmt-2(RNAi)*, *atf-6(lof)*; *pmt-2(RNAi)*, *ire-1(lof)*; *pmt-2(RNAi)*, and *pek-1(lof)*; *pmt-2(RNAi)* animals, respectively, using the gene ontology tool DAVID (Table S5) (Huang et al., 2007). Immune regulatory genes were found to be enriched in the upregulated categories of WT and *ire-1* animals (Fig. 4A,C). This is in agreement with a previous report where innate immunity was found to be modulated by *sams-1*, the methyl donor to *pmt-1* and *pmt-2* (Ding et al., 2015). Our data suggest that innate immune response is positively and negatively regulated by IRE-1 and PEK-1, respectively (Fig. 4C,D). As expected, GO terms related to ER stress were found to be enriched in the upregulated categories of WT and mutant animals when PC is depleted (Fig. 4A-D) (Ding et al., 2015). We also identified an enrichment of downregulated genes in WT related to translational initiation factors including *eif-1.A, eif-3.C* and *eif-3.E,* a characteristic effect of UPR activation (Ling et al., 2009, Long et al., 2002).

Protein tyrosine phosphatase activity is significantly regulated by ATF-6 upon LBS (GO ID: 0035335, n = 6, Benjamini *P* value 0.047) (Fig. 4B). This class of genes is activated in response to ER stress (Agouni et al., 2011). Transcriptional regulation (GO ID: 0006355, n = 49, Benjamini *P* value 3.3E-09) is enriched among IRE-1 dependent genes and supports the evidence that it alleviates ER stress by widespread transcriptional modification process (Fig. 4C) (Ng et al., 2000). In addition, genes involved in lipid and fatty acid processes were also enriched by IRE-1 and PEK-1 (Fig. 4C,D). Lastly, protein tyrosine phosphatase activity (GO ID: 0004725, n = 4, Benjamini *P* value = 0.039) is enriched by PEK-1, suggesting its involvement in protein modifications and cell signalling cascade during lipid bilayer stress (Fig. 4D) (Bettaieb et al., 2012). Interestingly, we observed upregulation of autophagy-related processes that are IRE-1 dependent shown in the volcano plot, where autophagy-related genes with at least 1.5-fold change and FDR *P* values less than 0.05 were displayed on the plot (Fig. 4 C,E). Crosstalk between the UPR and autophagy in the context of protein clearance has been well documented [for review see (Mizushima and Komatsu, 2011)].

IRE-1/XBP-1 axis regulates autophagy during UPR^{LBS}

To investigate if the autophagic process is activated during the UPR^{LBS}, we carried out an RNAi screen of autophagy-related genes. To decrease PC levels, WT worms were first subjected to 36 h of *pmt-2* RNAi followed by 5 days of autophagy-related gene RNAi treatment (Fig. 5A). Phenotypes following RNAi treatment were classified as 0 (little difference in growth and brood size), 1 (smaller brood size,

sick), and 2 (sterile, very sick) compared to vector control. The screen was carried out twice and scores were designated for both WT animals pre-treated with vector and *pmt-2* RNAi. A clone was classified as positive if the difference of the sum of *pmt-2* RNAi treatment to vector treatment is ≥ 3 (Table S6). From the 40 RNAi clones, 7 were found to induce development defects upon RNAi treatment compared to vector control (Fig. S5). As positive controls, we incorporated *ero-1* and *pmt-2* RNAis as either lead to developmental defects and sterility. The screen revealed that some autophagy-related genes are required during UPR^{LBS} and their absence contributes to the observed detrimental phenotypes. Identified genes include *atg-7* (orthologue of human ATG7, autophagosome conjugation), *atg-13* (orthologue of human ATG13, autophagosome formation), *bec-1* (orthologue of human Beclin1, vesicle nucleation), and *wdfy-3* (orthologue of human WDFY3, autophagy adaptor) (Melendez et al., 2003, Takacs-Vellai et al., 2005, Jia et al., 2007, Wang et al., 2018). Additionally, the screen has identified potential autophagy-related genes that are less characterised and prompt further investigation. These include *rsks-1* (orthologue of human RPS6KB1, negative regulator of autophagy), *sepa-1* (No human orthologue identified, P-granules-associated autophagy), and *trpp-8* (orthologue of human GSG1, autophagic processes).

To better understand the crosstalk between UPR^{LBS} and autophagy, we monitored the transcription levels of key autophagy-regulatory genes. Both *bec-1* and *lgg-1* (orthologue of human MAP1LC3, autophagosome formation) genes were found to be significantly upregulated in WT, *atf-6(lof)* and *pek-1(lof)* but not in *ire-1(lof)* compared to control upon *pmt-2* RNAi treatment (Fig. 5B,C). These results suggest that IRE-1 modulates *bec-1* and *lgg-1* expression during LBS. We validated that *bec-1* and *lgg-1* are both upregulated by tunicamycin as previously reported (Ogata et al., 2006). Once IRE-1 is activated, it cleaves *xbp-1* mRNA through an unconventional splicing. This is followed by the translation of the XBP-1 transcription factor which regulates a downstream signalling cascade (Walter and Ron, 2011, Ho et al., 2018) that modulates the expression of target genes including *hsp-3* during UPR^{LBS} (Fig. S6A). Thus, we monitored *bec-1 and lgg-1* mRNA levels in *xbp-1(lof)* treated with *pmt-2* RNAi. The upregulation of *bec-1* and *lgg-1* was abolished in *xbp-1(lof)* suggesting that XBP-1 modulates autophagy during UPR^{LBS} (Fig. 5D,E). Similar increase in mRNAs of *atg-18* (orthologue of human *WIPI*) and *epg-4* (orthologue of human *EI24*) were observed in *pmt-2(RNAi)* but not in *xbp-1(lof);pmt-2(RNAi)* animals (Fig. 5F,G) (Tian et al., 2010, Devkota et al., 2016). On the other hand, no significant transcriptional variations in *atg-4.1* (orthologue of human *ATG4*) and *atg-9* (orthologue of human *ATG9*) were observed, while *atg-16.2* (orthologue of human *ATG16L1*) was upregulated upon LBS in a XBP-1-independent manner (Fig. S6B-D). Altogether, these findings suggest that the UPR programme transcriptionally regulates a subset of autophagy genes during lipid bilayer stress.

To gain insight in autophagy flux, we used the autophagy reporter strain *plgg-1::gfp::lgg-1* in *eri-1* worms, which are highly sensitive to simultaneous treatment with two different RNAi (Melendez et al., 2003). We detected an increased number of GFP::LGG-1 puncta in intestinal tissues of *pmt-2(RNAi)* animals, but not in *ire-1* and *pmt-2* double RNAi treated animals (Figs 5H,I, S6E-G). These puncta are indicative of autophagosomes as spermidine treatment increased the number of GFP::LGG-1 puncta

(Jia et al., 2009). Next, we separated GFP::LGG-1 from its PE-conjugated form, GFP::LGG-1-PE, an autophagosomal marker (Kang et al., 2007). When entering the lysosome, GFP::LGG-1-PE is hydrolysed, releasing stable and free GFP (Hosokawa et al., 2006). Significant increases in GFP::LGG-1-PE as well as free GFP were observed in *pmt-2(RNAi)* but not in *ire-1(RNAi)*;*pmt-2(RNAi)* (Fig. 5J,K). Together, these results indicate that autophagy is modulated by the IRE-1/XBP-1 axis upon UPR^{LBS}.

DISCUSSION

Lipid perturbation refers to excessive accumulation of lipids in tissues including liver, pancreas and adipose (Hotamisligil and Erbay, 2008, Rinella and Sanyal, 2015). Dysfunctional UPR and apoptotic pathways resulting from this lipotoxicity ultimately lead to disease outcomes. To better understand the role of the UPR during lipid bilayer stress and the consequence of a compromised UPR programme, several studies have been conducted, focusing on their interconnection. As it is required for normal fatty acid synthesis as well as the regulation of very low-density lipoprotein (VLDL) assembly and secretion, *XBP1* ablation leads to hypolipidemia in mice due to an abnormal decrease in plasma levels of TG and cholesterol (Lee et al., 2008, So et al., 2012, Wang et al., 2012). High dietary carbohydrate is sufficient to increase FAs and cholesterol synthesis through XBP1 (Lee et al., 2008). Consequently, XBP1 is required to channel excess carbohydrate into lipids as its absence leads to insulin resistance in obese mice (Ozcan et al., 2004). XBP1 is also required to modulate phospholipid synthesis to expand the ER membrane network during proteotoxic stress, a process that is proposed to accommodate the increased load of misfolded proteins (Sriburi et al., 2004). The UPR modulates lipid metabolism-related genes and the absence of its sole regulator in yeast, Ire1, confers auxotrophy of inositol, a building block of phospholipids (Cox et al., 1993). We have previously shown that Ire1 is essential for cell survival during lipid bilayer stress, thereby highlighting the important role of the UPR to overcome lipotoxicity in yeast (Thibault et al., 2012). The UPR sensor PERK also plays a role in pathogenesis from lipotoxicity. Lipotoxicity-induced CHOP, the downstream target gene of PERK, promotes hepatic inflammation by activating the NK-κB pathway, thus promoting NASH and type 2 diabetes (Cunha et al., 2008, Willy et al., 2015). The ablation of ATF6, the third UPR sensor, induces NASH due to dysregulated lipid biosynthesis in mice upon tunicamycin treatment (Yamamoto et al., 2010). Thus, the three branches of the UPR are intimately linked to lipid homeostasis but their respective roles during lipid bilayer stress in comparison to proteotoxic stress remains elusive. Here, we took a systematic global approach to determine genes that are UPR-regulated specifically from lipid bilayer stress.

To introduce lipid bilayer stress in *C. elegans*, we opted to genetically attenuate *pmt-2* which is required for *de novo* PC biosynthesis (Fig. 1A). A similar approach has been used by other groups to mimic the physiological conditions associated to NAFLD in *C. elegans* (Walker et al., 2011, Ding et al., 2015, Smulan et al., 2016). Both required for *de novo* PC biosynthesis, *pmt-2* and *sams-1* depletion leads to enlarged lipid droplets in worms (Li et al., 2004). Generally, perturbing PC levels affects the abundance and size of lipid droplets, serving as a compensatory response to lipid bilayer stress that results in the

channelling of excess neutral lipids, triacylglycerol and sterol, into lipid droplets (LDs) (Guo et al., 2008, Li et al., 2011, Walker et al., 2011).

Decreased hepatic PC in mice (Walkey et al., 1998, Ozcan et al., 2004, Li et al., 2006, Fu et al., 2011b) and dietary deficiency of choline in humans are both associated with hepatic steatosis (Buchman et al., 1995, Gao et al., 2016). Initially, we subjected young adult worms to *pmt-2* RNAi for two days. However, no significant decrease in PC level was observed (data not shown). This could be due to the slow turnover of phospholipids in *C. elegans*. The absence of cell division in adult worms might not require the rapid synthesis of new membrane lipids thus genetic ablation of *pmt-2* may have little or no effect on PC levels (Kipreos, 2005). Thus, L1 stage worms treated with *pmt-2* RNAi were utilised as UPR^{LBS} model. Nonetheless, these conditions were sufficient to drastically induce lipid bilayer stress, lipid storage, and to strongly activate the UPR, all hallmark of NAFLD (Figs 1, 2, S1-S3). Using this approach, we interrogated the role of each UPR branch during lipid bilayer stress-induced ER stress.

We employed *C. elegans* for its well-conserved UPR pathways and relative simplicity for genetic analysis. We examined the individual effects of *atf-6*, *ire-1*, and *pek-1* deficiency *in vivo*. Interestingly, ER stress induced by unfolded protein accumulation and lipid bilayer stress were found to be distinct from each other (Hou et al., 2014, Lajoie et al., 2012). The global transcriptomic analysis of UPR mutants subjected to lipid bilayer stress in comparison to proteotoxic-induced ER stress in WT allowed us to identify genes that are specifically regulated from the UPR^{LBS} but not the UPR^{PT} (Fig. 3). To our knowledge, this is the first report identifying specific UPR-regulated genes induced by lipid bilayer stress but not proteotoxic stress. Our data show that a number of genes regulated by the UPR transducers are specific to lipid bilayer stress, while a smaller number of genes are commonly modulated under proteotoxic and lipid stress. As expected, lipid bilayer stress-induced ER stress leads to altered gene regulation and protein modification processes through ATF-6, IRE-1, and PEK-1 (Figs 3, 4). IRE-1 is the most conserved UPR transducer from yeast to mammals and it regulates the largest number of genes among the three UPR transducers (Fig. 3B).

Our autophagy screening revealed that autophagy is essential during lipid bilayer stress, suggesting its important role in regulating lipid metabolism. The change in cellular lipid landscape is at least partially mediated by autophagy, through the IRE-1/XBP-1 axis (Figs 4, 5). Generally considered a cytoprotective response, autophagy can be modulated from ER stress. PERK has been reported to modulate autophagy by phosphorylating eIF2α resulting in a general translational inhibition (Matsumoto et al., 2013, Avivar-Valderas et al., 2011, Fujita et al., 2007, Kouroku et al., 2007). In parallel, PERK was also reported to regulate autophagy through the transcription factor ATF4 (orthologue of ATF-5) (Carra et al., 2009, Dever, 2002, Talloczy et al., 2002). Likewise, IRE1 modulates autophagy, independently of XBP1, by activating the Jun N-terminal kinase (JNK) pathway (Younce and Kolattukudy, 2012, Vidal et al., 2012, Pattingre et al., 2009, Wei et al., 2008b, Wei et al., 2008a, Ogata et al., 2006). Autophagy has additionally been reported to be activated (Younce and Kolattukudy, 2012)

or inhibited (Vidal et al., 2012) by the IRE1/XBP1 axis (Adolph et al., 2013, Zhao et al., 2013, Hetz et al., 2009).

Muting the UPR during lipid bilayer stress revealed that the IRE-1/XBP-1 axis specifically modulates autophagy (Fig. 6). Our findings also demonstrate that a subset of autophagy genes is essential for organismal health during LBS (Figs 5A, S5 and Table S6). Considering the important role of lipid homeostasis and how its impairment contributes to the pathology of metabolic diseases, our data revealed the important role of a functional UPR programme to regulate autophagy and consequently maintain cellular homeostasis. As increasing evidences suggest that dampened autophagy contributes to a myriad of pathological outcomes (Mizushima et al., 2008, Singh et al., 2009), the autophagy process might be a useful target for therapeutic development in metabolic diseases.

MATERIALS AND METHODS

Statistics

Error bars indicate standard error of the mean (s.e.m.), calculated from at least three biological replicates, unless otherwise indicated. *P* values were calculated using one-way ANOVA with Tukey's post hoc test, unless otherwise indicated and reported as *P* values with 4 significant digits in the figures. All statistical tests were performed using GraphPad Prism 7 software.

C. elegans strains and RNAi constructs

All strains were grown at 20°C using standard *C. elegans* methods as previously described (Brenner, 1974, Stiernagle, 2006). Nematode growth media (NGM) agar plates were seeded with *Escherichia coli* strain OP50 for normal growth and with HT115 bacteria for RNAi feeding. RNAi feeding was performed as previously described (Timmons and Fire, 1998), and the RNAi library was obtained from the Fire lab (Fire et al., 1998). The plasmids were sequenced to confirm their identity. Wild-type N2 Bristol, *atf-6*(ok551), *ire-1*(ok799), *pek-1*(ok275), *pmt-2*(vc1952), *phsp4::gfp*(sj4005), *xbp-1(lof);phsp-4::gfp*(sj17), *eri-1(mg366)* and *plgg-1::gfp::lgg-1*(adIs2122) were obtained from *Caenorhabditis* Genetic Center (CGC). The *eri-1;plgg-1::gfp::lgg-1* reporter strain was obtained by crossing *eri-1* worms to *plgg-1::gfp::lgg-1* as previously described (Fay, 2006).

RNAi by feeding

RNAi was carried out as previously described (Timmons and Fire, 1998). Briefly, HT115 bacteria harbouring pL4440 plasmids were grown in LB medium containing 100 µg/ml ampicillin at 37°C until log phase (OD_{600} 0.6) and seeded onto NGM agar plates containing 50 µg/ml carbenicillin and 1 mM isopropyl β-D-1-thiogalactopyranoside (IPTG). Gravid adult worms were treated with hypochlorite and eggs were hatched overnight in M9 medium at 20°C to obtain L1 synchronised worms. Hatched L1 larvae were transferred to RNAi agar plates and grown until L4 larval to young adult stages. L4/young adult worms were harvested and incubated with 25 µg/ml tunicamycin in M9 medium for 4 hours at 20°C followed by M9 washes when indicated. To measure body length, worms were transferred to 6

cm NGM plates without bacteria. Bright field images were acquired with a dissecting microscope (Nikon SMZ1500) fitted with a JVC digital camera at 100X magnification. Length measurements were performed in Fiji with the WormSizer plugin (Moore et al., 2013). For double RNAi feeding, worms were fed with equal amount of HT115 bacteria harbouring pL4440 plasmids and the efficacy of gene silencing was assessed by quantitative real-time PCR.

Quantitative real-time PCR

Ten thousand L4/young adult worms were collected, resuspended in water and lysed with a motorised pestle homogeniser. Total RNA was isolated using TRIzol reagent (Thermo Fisher, Waltham, MA) and subsequently purified using RNeasy Mini (Qiagen, Venlo, Netherlands) columns following manufacturer's protocols. DNase treatment in columns was carried out with RNase-Free DNase (Qiagen, Venlo, Netherlands) following manufacturer's protocol. cDNA was synthesised from 2 µg of total RNA using RevertAid Reverse Transcriptase (Thermo Fisher, Waltham, MA) following manufacturer's protocol. SYBR Green quantitative real-time PCR (qPCR) experiments were performed following the manufacturer's protocol using a QuantStudio 6 Flex Real-time PCR system (Applied Biosystems, Waltham, MA). Thirty nanograms of cDNA and 50 nM of paired-primer mix were used for each reaction. Relative mRNA was determined with the comparative Ct method (ΔΔCt) normalised to housekeeping gene *act-1*. Oligonucleotide primers used are listed in Table S1.

Lipid extraction and phospholipid analysis

Approximately 10,000 L4 to young adult worms were harvested and washed thoroughly with M9 buffer, lysed with 1 mm silica beads by bead beating and subsequently lyophilised overnight (Virtis). All subsequent steps were carried out at 4°C. Total lipids were extracted from dried samples with chloroform:methanol (2:1) and concentrated. Total lipid extracts and POPE (1-palmitoyl-2-oleoyl-sn-glycero-3-phosphoethanolamine; 16:0-18:1n9 PE; Avanti Polar Lipids, Alabaster, AL) / DOPC (1,2-dioleoyl-sn-glycero-3-phosphocholine; 18:1n9 PC; Avanti Polar Lipids, Alabaster, AL) standard mix were spotted on HPTLC Silica gel 60 plates using Linomat 5 (CAMAG) and separated with chloroform:methanol:acetic acid:acetone:water (35:25:4:14:2). Phospholipids were visualised under long-wave ultraviolet (λ = 340 nm) by spraying 0.05 mg/ml of primuline dye in acetone:water (80:20) onto the dried plates. Spots corresponding to PE and PC were scraped off the silica plates and transferred into 2 ml glass tubes. One hundred microliters of 1 mM C15:0 (pentadecanoic acid) was added to the tubes containing silica-bound phospholipids as an internal standard. The phospholipids were hydrolysed and esterified to fatty acid methyl esters (FAME) with 300 µl of 1.25 M HCl-methanol for 1 h at 80°C. FAMEs were extracted three times with 1 ml of hexane. Combined extracts were dried under nitrogen, resuspended in 100 µl hexane. FAMEs were separated by gas chromatography with flame ionization detector (GC-FID) (GC-2014; Shimadzu, Kyoto, Japan) using an ULBON HR-SS-10 50 m x 0.25 mm column (Shinwa, Tokyo, Japan). Supelco 37 component FAME mix was used to identify corresponding fatty acids (Sigma-Aldrich, St. Louis, MO). Data were normalised using the internal standard C15:0 and worm dry weight.

Lipid droplets analysis by Sudan Black

Following RNAi feeding, lipid droplets of L4 worms were stained with Sudan Black B (Sigma-Aldrich, St. Louis, MO) as described previously with few modifications (Ogg and Ruvkun, 1998). Briefly, worms were fixed in 1% paraformaldehyde in M9 buffer for 30 minutes at room temperature, followed by three freeze-thaw cycles using liquid nitrogen. Worms were washed once with M9 and gradually dehydrated with 25%, 50% and 70% ethanol. Subsequently, fixed worms were stained with 50% saturated Sudan Black B in 70% ethanol (filtered with 0.22 µm membrane) for 30 minutes at room temperature with rocking. Stained worms were washed once with 25% ethanol for 30 minutes with rocking. Worms were mounted on a 2% agarose pads for imaging. Brightfield images of worms were taken with DMi8 inverted epifluorescence microscope (Leica, Wetzlar, Germany) with 20x and 63x objective lenses. To quantify lipid droplets, TIFF images taken at 63x magnification were converted to 8-bit grayscale, followed by background subtraction and thresholding with Fiji imaging software. Lipid droplets were divided into three size groups based on the diameter of LDs: small (0.8 - 3 µM), medium (3.1 - 6 µM) and large (> 6 µM). Percentage of LDs per size group against the sum of measured LDs per condition was presented.

Spermidine treatment

Worms at L4 stage were collected in M9 buffer and treated with 1 mM spermidine (Sigma-Aldrich, St. Louis, MO) for 16 h at 20°C with shaking. Worms were then washed 3 times with M9 buffer and harvested for downstream experiments.

Immunoblotting

Worms were collected, washed in M9 buffer and subsequently lysed in RIPA buffer (50 mM Tris, 150 mM NaCl, 1% NP-40, 0.1% SDS, 2 mM EDTA, pH 8.0 and 0.5% sodium deoxycholate) with protease inhibitor cocktail (Roche, Basel, Switzerland) by bead beating three times for 30 seconds at 6,500 RPM with the samples chilled on ice between the homogenization steps. Samples were then centrifuged at 10,000 x *g* for 5 minutes at 4°C to remove debris. Cleared lysate protein concentration was measured using the BCA Assay Kit (Thermo Fisher, Waltham, MA). Sixty micrograms and 80 µg of total proteins were loaded into 10% SDS-PAGE to detect free GFP and GFP::LGG-1, respectively, transferred to nitrocellulose membranes and stained with REVERT Total Protein Stain (Li-COR Biosciences, Lincoln, NE) for normalization. Membranes were blocked for 1 h with Odyssey Blocking Buffer TBS (Li-COR Biosciences, Lincoln, NE) at room temperature, incubated with 1:1,000 of monoclonal anti-GFP overnight at 4°C (Roche, catalogue number 11814460001), washed, and incubated with 1:10,000 of IRDye 800CW anti-mouse IgG (Li-COR Biosciences, Lincoln, NE, catalogue number 925-32210). Membranes were washed and scanned with an Odyssey CLx Imaging System (Li-COR Biosciences, Lincoln, NE).

Quantification of autophagic vesicles

To quantify autophagic vesicles, *eri-1;lgg-1p::gfp::lgg-1* worms were immobilised in M9 containing 0.5 M NaN_3 and mounted on 2% agarose pad and imaged using LSM Zeiss 710 scanning confocal

microscope (Zeiss, Oberkochen, Germany). GFP excitation and emission wavelengths were adjusted to 493 and 517 nm, respectively, to reduce autofluorescence. Z-stacks were acquired with a 63x objective of 0.6 μM thickness. Line average scanning was set to 8 times to increase signal-to-noise ratio. Maximum intensity projection was acquired from the z-stack images with ZEN software (Zeiss, Oberkochen, Germany). GFP positive puncta were quantified in one 1000 μm^2 area around the anterior intestines with ZEN software.

DNA microarray

Three independent populations of WT, *atf-6(lof), ire-1(lof), pek-1(lof)* and *pmt-2(lof)* worms were synchronised by hypochlorite treatment. L1 stage animals were treated with *pmt-2* RNAi or pL4440 empty vector for 48 h. Next, total RNA from the treated worms was isolated as described above. RNA quality control for microarray analysis was carried out using Agilent 2100 Bioanalyzer (Agilent Technologies, Santa Clara, CA). RNA samples with RIN score > 9.5 were deemed suitable for microarrays. The cDNAs were then synthesised from 100 ng of total RNA, purified, fragmented and hybridised to GeneChip C. elegans Gene 1.0 ST Arrays. Differentially expressed genes were identified using Affymetrix Transcriptome Analysis Console (TAC) 3.0 software. Threshold for selecting differentially expressed genes were set at a difference of more than 1.5-fold and one-way between subjects ANOVA *P* value < 0.05. GOrilla (http://cbl-gorilla.cs.technion.ac.il/) (Eden et al., 2009), REViGO (http://revigo.irb.hr/) (Supek et al., 2011), and DAVID (https://david.ncifcrf.gov/) (Huang et al., 2007) were used for GO terms analysis. Heat maps in the figures were generated using R Studio. Venn diagrams were generated using the following generator (http://bioinfo.genotoul.fr/jvenn/example.html). For gene expression analysis, normalised and log transformed array data were imported to Cluster 3.0 for fold cut-off and hierarchical clustering. Genes were filtered to obtain those with a significant change in gene expression (fold change > 1.5 between RNAi treated and untreated samples and $P < 0.05$). The filtered data set was hierarchically clustered based on average linkage and Pearson correlation method, and the output was displayed in TreeView. Quantitative real-time PCR was performed to verify mRNA expression of selected gene targets.

RNAi screening of autophagy-related genes

RNAi screen was carried out as previously described with minor modifications (Lehner et al., 2006). Briefly, L1 larval stage animals were synchronised by hypochlorite treatment and exposed to *pmt-2 RNAi* on NGM agar plates for 36 h. Thereafter, worms were washed thrice with M9 and five to ten worms were seeded into a 96-well plate containing RNAi clones of autophagy-related functions. Control RNAi plates comprised worms exposed to pL4440 empty vector for 48 h and subsequently seeded into 96-well plates containing the same RNAi clones as above. Phenotypes of the worms were monitored over a five-day period. Phenotypes were compared to control RNAi plates where the worms were scored with sterility and reduced body size semi-quantitatively on a scale from 0 (wild-type) to 2 (100% sterility or stunted growth) (Lehner et al., 2006).

ACKNOWLEDGEMENTS

We are grateful to Drs Fumio Motegi, Jean-Claude Labbé and Ronen Zaidel-Bar for providing reagents and technical support to introduce *C. elegans* as a new model system in the laboratory. Some strains were provided by the CGC, which is funded by NIH Office of Research Infrastructure Programs (P40 OD010440). We thank Peter Shyu Jr. for critical reading of the manuscript.

COMPETING INTERESTS

The authors declare no competing or financial interests.

AUTHOR CONTRIBUTIONS

Conceptualisation: G.T; Methodology: K.J.H., W.L., C.B.C., and G.T.; Formal Analysis: K.J.H.; Investigation: K.J.H., W.L., and C.B.C.; Resources: K.J.H. and W.L.; Writing – Original Draft: K.J.H. and G.T.; Writing – Review & Editing: K.J.H., W.L., C.B.C., and G.T.; Funding Acquisition: K.J.H. and G.T.

FUNDING

This work was supported by the Nanyang Assistant Professorship programme from Nanyang Technological University, the Singapore Ministry of Education Academic Research Fund Tier 1 (2016-T1-001-078), and the Nanyang Technological University Research Scholarship to J.H.K. (predoctoral fellowship).

DATA AVAILABILITY

The DNA microarray data discussed in this publication was deposited in NCBI's Gene Expression Onmibus (GEO) under series number GSE99763.

REFERENCES

ACOSTA-ALVEAR, D., ZHOU, Y., BLAIS, A., TSIKITIS, M., LENTS, N. H., ARIAS, C., LENNON, C. J., KLUGER, Y. & DYNLACHT, B. D. 2007. XBP1 controls diverse cell type- and condition-specific transcriptional regulatory networks. *Mol Cell,* 27**,** 53-66.

ADOLPH, T. E., TOMCZAK, M. F., NIEDERREITER, L., KO, H. J., BOCK, J., MARTINEZ-NAVES, E., GLICKMAN, J. N., TSCHURTSCHENTHALER, M., HARTWIG, J., HOSOMI, S., FLAK, M. B., CUSICK, J. L., KOHNO, K., IWAWAKI, T., BILLMANN-BORN, S., RAINE, T., BHARTI, R., LUCIUS, R., KWEON, M. N., MARCINIAK, S. J., CHOI, A., HAGEN, S. J., SCHREIBER, S., ROSENSTIEL, P., KASER, A. & BLUMBERG, R. S. 2013. Paneth cells as a site of origin for intestinal inflammation. *Nature,* 503**,** 272-6.

AGOUNI, A., MODY, N., OWEN, C., CZOPEK, A., ZIMMER, D., BENTIRES-ALJ, M., BENCE, K. K. & DELIBEGOVIC, M. 2011. Liver-specific deletion of protein tyrosine phosphatase (PTP) 1B improves obesity- and pharmacologically induced endoplasmic reticulum stress. *Biochem J,* 438**,** 369-78.

ARENDT, B. M., MA, D. W., SIMONS, B., NOURELDIN, S. A., THERAPONDOS, G., GUINDI, M., SHERMAN, M. & ALLARD, J. P. 2013. Nonalcoholic fatty liver disease is associated with lower hepatic and erythrocyte ratios of phosphatidylcholine to phosphatidylethanolamine. *Appl Physiol Nutr Metab,* 38**,** 334-40.

AVIVAR-VALDERAS, A., SALAS, E., BOBROVNIKOVA-MARJON, E., DIEHL, J. A., NAGI, C., DEBNATH, J. & AGUIRRE-GHISO, J. A. 2011. PERK integrates autophagy and oxidative stress responses to promote survival during extracellular matrix detachment. *Mol Cell Biol,* 31**,** 3616-29.

BETTAIEB, A., MATSUO, K., MATSUO, I., WANG, S., MELHEM, R., KOROMILAS, A. E. & HAJ, F. G. 2012. Protein tyrosine phosphatase 1B deficiency potentiates PERK/eIF2alpha signaling in brown adipocytes. *PLoS One,* 7**,** e34412.

BRAAKMAN, I. & BULLEID, N. J. 2011. Protein folding and modification in the mammalian endoplasmic reticulum. *Annu Rev Biochem,* 80**,** 71-99.

BRENDZA, K. M., HAAKENSON, W., CAHOON, R. E., HICKS, L. M., PALAVALLI, L. H., CHIAPELLI, B. J., MCLAIRD, M., MCCARTER, J. P., WILLIAMS, D. J., HRESKO, M. C. & JEZ, J. M. 2007. Phosphoethanolamine N-methyltransferase (PMT-1) catalyses the first reaction of a new pathway for phosphocholine biosynthesis in Caenorhabditis elegans. *Biochem J,* 404**,** 439-48.

BRENNER, S. 1974. The genetics of Caenorhabditis elegans. *Genetics,* 77**,** 71-94.

BUCHMAN, A. L., DUBIN, M. D., MOUKARZEL, A. A., JENDEN, D. J., ROCH, M., RICE, K. M., GORNBEIN, J. & AMENT, M. E. 1995. Choline deficiency: a cause of hepatic steatosis during parenteral nutrition that can be reversed with intravenous choline supplementation. *Hepatology,* 22**,** 1399-403.

CALFON, M., ZENG, H., URANO, F., TILL, J. H., HUBBARD, S. R., HARDING, H. P., CLARK, S. G. & RON, D. 2002. IRE1 couples endoplasmic reticulum load to secretory capacity by processing the XBP-1 mRNA. *Nature,* 415**,** 92-6.

CARRA, S., BRUNSTING, J. F., LAMBERT, H., LANDRY, J. & KAMPINGA, H. H. 2009. HspB8 participates in protein quality control by a non-chaperone-like mechanism that requires eIF2{alpha} phosphorylation. *J Biol Chem,* 284**,** 5523-32.

COX, J. S., SHAMU, C. E. & WALTER, P. 1993. Transcriptional induction of genes encoding endoplasmic reticulum resident proteins requires a transmembrane protein kinase. *Cell,* 73**,** 1197-206.

COX, J. S. & WALTER, P. 1996. A novel mechanism for regulating activity of a transcription factor that controls the unfolded protein response. *Cell,* 87**,** 391-404.

CUNHA, D. A., HEKERMAN, P., LADRIERE, L., BAZARRA-CASTRO, A., ORTIS, F., WAKEHAM, M. C., MOORE, F., RASSCHAERT, J., CARDOZO, A. K., BELLOMO, E., OVERBERGH, L., MATHIEU, C., LUPI, R., HAI, T., HERCHUELZ, A., MARCHETTI, P., RUTTER, G. A., EIZIRIK, D. L. & CNOP, M. 2008. Initiation and execution of lipotoxic ER stress in pancreatic beta-cells. *J Cell Sci,* 121**,** 2308-18.

DEVER, T. E. 2002. Gene-specific regulation by general translation factors. *Cell,* 108**,** 545-56.

DEVKOTA, S., JEONG, H., KIM, Y., ALI, M., ROH, J. I., HWANG, D. & LEE, H. W. 2016. Functional characterization of EI24-induced autophagy in the degradation of RING-domain E3 ligases. *Autophagy,* 12**,** 2038-2053.

DING, W., SMULAN, L. J., HOU, N. S., TAUBERT, S., WATTS, J. L. & WALKER, A. K. 2015. s-Adenosylmethionine Levels Govern Innate Immunity through Distinct Methylation-Dependent Pathways. *Cell Metab,* 22**,** 633-45.

DOWD, S. R., BIER, M. E. & PATTON-VOGT, J. L. 2001. Turnover of phosphatidylcholine in Saccharomyces cerevisiae. The role of the CDP-choline pathway. *J Biol Chem,* 276**,** 3756-63.

DOYCHEVA, I., WATT, K. D., RIFAI, G., ABOU MRAD, R., LOPEZ, R., ZEIN, N. N., CAREY, W. D. & ALKHOURI, N. 2017. Increasing Burden of Chronic Liver Disease Among Adolescents and Young Adults in the USA: A Silent Epidemic. *Dig Dis Sci,* 62**,** 1373-1380.

EDEN, E., NAVON, R., STEINFELD, I., LIPSON, D. & YAKHINI, Z. 2009. GOrilla: a tool for discovery and visualization of enriched GO terms in ranked gene lists. *BMC Bioinformatics,* 10**,** 48.

ERICSON, M. C., GAFFORD, J. T. & ELBEIN, A. D. 1977. Tunicamycin inhibits GlcNAc-lipid formation in plants. *J Biol Chem,* 252**,** 7431-3.

FAY, D. 2006. Genetic mapping and manipulation: chapter 1--Introduction and basics. *WormBook***,** 1-12.

FIRE, A., XU, S., MONTGOMERY, M. K., KOSTAS, S. A., DRIVER, S. E. & MELLO, C. C. 1998. Potent and specific genetic interference by double-stranded RNA in Caenorhabditis elegans. *Nature,* 391**,** 806-11.

FU, S., YANG, L., LI, P., HOFMANN, O., DICKER, L., HIDE, W., LIN, X., WATKINS, S. M., IVANOV, A. R. & HOTAMISLIGIL, G. S. 2011a. Aberrant lipid metabolism disrupts calcium homeostasis causing liver endoplasmic reticulum stress in obesity. *Nature,* 473**,** 528-31.

FU, S., YANG, L., LI, P., HOFMANN, O., DICKER, L., HIDE, W., LIN, X., WATKINS, S. M., IVANOV, A. R. & HOTAMISLIGIL, G. S. 2011b. Aberrant lipid metabolism disrupts calcium homeostasis causing liver endoplasmic reticulum stress in obesity. *Nature,* 473**,** 528-531.

FUJITA, E., KOUROKU, Y., ISOAI, A., KUMAGAI, H., MISUTANI, A., MATSUDA, C., HAYASHI, Y. K. & MOMOI, T. 2007. Two endoplasmic reticulum-associated degradation (ERAD) systems for the novel variant of the mutant dysferlin: ubiquitin/proteasome ERAD(I) and autophagy/lysosome ERAD(II). *Hum Mol Genet,* 16**,** 618-29.

GAO, X., WANG, Y., RANDELL, E., PEDRAM, P., YI, Y., GULLIVER, W. & SUN, G. 2016. Higher Dietary Choline and Betaine Intakes Are Associated with Better Body Composition in the Adult Population of Newfoundland, Canada. *PLoS One,* 11**,** e0155403.

GUO, Y., WALTHER, T. C., RAO, M., STUURMAN, N., GOSHIMA, G., TERAYAMA, K., WONG, J. S., VALE, R. D., WALTER, P. & FARESE, R. V. 2008. Functional genomic screen reveals genes involved in lipid-droplet formation and utilization. *Nature,* 453**,** 657-61.

HALBLEIB, K., PESEK, K., COVINO, R., HOFBAUER, H. F., WUNNICKE, D., HANELT, I., HUMMER, G. & ERNST, R. 2017. Activation of the Unfolded Protein Response by Lipid Bilayer Stress. *Mol Cell,* 67**,** 673-684 e8.

HAN, J. & KAUFMAN, R. J. 2016. The role of ER stress in lipid metabolism and lipotoxicity. *J Lipid Res,* 57**,** 1329-38.

HARDING, H. P., ZHANG, Y., ZENG, H., NOVOA, I., LU, P. D., CALFON, M., SADRI, N., YUN, C., POPKO, B., PAULES, R., STOJDL, D. F., BELL, J. C., HETTMANN, T., LEIDEN, J. M. & RON, D. 2003. An integrated stress response regulates amino acid metabolism and resistance to oxidative stress. *Mol Cell,* 11**,** 619-33.

HETZ, C., THIELEN, P., MATUS, S., NASSIF, M., COURT, F., KIFFIN, R., MARTINEZ, G., CUERVO, A. M., BROWN, R. H. & GLIMCHER, L. H. 2009. XBP-1 deficiency in the nervous system protects against amyotrophic lateral sclerosis by increasing autophagy. *Genes Dev,* 23**,** 2294-306.

HO, N., XU, C. & THIBAULT, G. 2018. From the unfolded protein response to metabolic diseases - lipids under the spotlight. *J Cell Sci,* 131.

HORL, G., WAGNER, A., COLE, L. K., MALLI, R., REICHER, H., KOTZBECK, P., KOFELER, H., HOFLER, G., FRANK, S., BOGNER-STRAUSS, J. G., SATTLER, W., VANCE, D. E. & STEYRER, E. 2011. Sequential synthesis and methylation of phosphatidylethanolamine promote lipid droplet biosynthesis and stability in tissue culture and in vivo. *J Biol Chem,* 286**,** 17338-50.

HOSOKAWA, N., HARA, Y. & MIZUSHIMA, N. 2006. Generation of cell lines with tetracycline-regulated autophagy and a role for autophagy in controlling cell size. *FEBS Lett,* 580**,** 2623-9.

HOTAMISLIGIL, G. S. & ERBAY, E. 2008. Nutrient sensing and inflammation in metabolic diseases. *Nat Rev Immunol,* 8**,** 923-34.

HOU, N. S., GUTSCHMIDT, A., CHOI, D. Y., PATHER, K., SHI, X., WATTS, J. L., HOPPE, T. & TAUBERT, S. 2014. Activation of the endoplasmic reticulum unfolded protein response by lipid disequilibrium without disturbed proteostasis in vivo. *Proc Natl Acad Sci U S A,* 111**,** E2271-80.

HUANG, D. W., SHERMAN, B. T., TAN, Q., COLLINS, J. R., ALVORD, W. G., ROAYAEI, J., STEPHENS, R., BASELER, M. W., LANE, H. C. & LEMPICKI, R. A. 2007. The DAVID Gene Functional Classification Tool: a novel biological module-centric algorithm to functionally analyze large gene lists. *Genome Biol,* 8**,** R183.

JIA, K., HART, A. C. & LEVINE, B. 2007. Autophagy genes protect against disease caused by polyglutamine expansion proteins in Caenorhabditis elegans. *Autophagy,* 3**,** 21-5.

JIA, K., THOMAS, C., AKBAR, M., SUN, Q., ADAMS-HUET, B., GILPIN, C. & LEVINE, B. 2009. Autophagy genes protect against Salmonella typhimurium infection and mediate insulin signaling-regulated pathogen resistance. *Proc Natl Acad Sci U S A,* 106**,** 14564-9.

KANG, C., YOU, Y. J. & AVERY, L. 2007. Dual roles of autophagy in the survival of Caenorhabditis elegans during starvation. *Genes Dev,* 21**,** 2161-71.

KIM, M. H., AYDEMIR, T. B., KIM, J. & COUSINS, R. J. 2017. Hepatic ZIP14-mediated zinc transport is required for adaptation to endoplasmic reticulum stress. *Proc Natl Acad Sci U S A,* 114**,** E5805-E5814.

KIPREOS, E. T. 2005. C. elegans cell cycles: invariance and stem cell divisions. *Nat Rev Mol Cell Biol,* 6**,** 766-76.

KOUROKU, Y., FUJITA, E., TANIDA, I., UENO, T., ISOAI, A., KUMAGAI, H., OGAWA, S., KAUFMAN, R. J., KOMINAMI, E. & MOMOI, T. 2007. ER stress (PERK/eIF2alpha phosphorylation) mediates the polyglutamine-induced LC3 conversion, an essential step for autophagy formation. *Cell Death Differ,* 14**,** 230-9.

LAGACE, T. A. & RIDGWAY, N. D. 2013. The role of phospholipids in the biological activity and structure of the endoplasmic reticulum. *Biochim Biophys Acta,* 1833**,** 2499-510.

LAJOIE, P., MOIR, R. D., WILLIS, I. M. & SNAPP, E. L. 2012. Kar2p availability defines distinct forms of endoplasmic reticulum stress in living cells. *Mol Biol Cell,* 23**,** 955-64.

LEE, A. H., SCAPA, E. F., COHEN, D. E. & GLIMCHER, L. H. 2008. Regulation of hepatic lipogenesis by the transcription factor XBP1. *Science,* 320**,** 1492-6.

LEHNER, B., TISCHLER, J. & FRASER, A. G. 2006. RNAi screens in Caenorhabditis elegans in a 96-well liquid format and their application to the systematic identification of genetic interactions. *Nat Protoc,* 1**,** 1617-20.

LI, Y., GE, M., CIANI, L., KURIAKOSE, G., WESTOVER, E. J., DURA, M., COVEY, D. F., FREED, J. H., MAXFIELD, F. R., LYTTON, J. & TABAS, I. 2004. Enrichment of endoplasmic reticulum with cholesterol inhibits sarcoplasmic-endoplasmic reticulum calcium ATPase-2b activity in parallel with increased order of membrane lipids: implications for depletion of endoplasmic reticulum calcium stores and apoptosis in cholesterol-loaded macrophages. *J Biol Chem,* 279**,** 37030-9.

LI, Y., NA, K., LEE, H. J., LEE, E. Y. & PAIK, Y. K. 2011. Contribution of sams-1 and pmt-1 to lipid homoeostasis in adult Caenorhabditis elegans. *J Biochem,* 149**,** 529-38.

LI, Z., AGELLON, L. B., ALLEN, T. M., UMEDA, M., JEWELL, L., MASON, A. & VANCE, D. E. 2006. The ratio of phosphatidylcholine to phosphatidylethanolamine influences membrane integrity and steatohepatitis. *Cell Metab,* 3**,** 321-31.

LI, Z., AGELLON, L. B. & VANCE, D. E. 2005. Phosphatidylcholine homeostasis and liver failure. *J Biol Chem,* 280**,** 37798-802.

LING, J., CHABA, T., ZHU, L. F., JACOBS, R. L. & VANCE, D. E. 2012. Hepatic ratio of phosphatidylcholine to phosphatidylethanolamine predicts survival after partial hepatectomy in mice. *Hepatology,* 55**,** 1094-102.

LING, J., REYNOLDS, N. & IBBA, M. 2009. Aminoacyl-tRNA synthesis and translational quality control. *Annu Rev Microbiol,* 63**,** 61-78.

LONG, X., SPYCHER, C., HAN, Z. S., ROSE, A. M., MULLER, F. & AVRUCH, J. 2002. TOR deficiency in C. elegans causes developmental arrest and intestinal atrophy by inhibition of mRNA translation. *Curr Biol,* 12**,** 1448-61.

MATSUMOTO, H., MIYAZAKI, S., MATSUYAMA, S., TAKEDA, M., KAWANO, M., NAKAGAWA, H., NISHIMURA, K. & MATSUO, S. 2013. Selection of autophagy or apoptosis in cells exposed to ER-stress depends on ATF4 expression pattern with or without CHOP expression. *Biol Open,* 2**,** 1084-90.

MELENDEZ, A., TALLOCZY, Z., SEAMAN, M., ESKELINEN, E. L., HALL, D. H. & LEVINE, B. 2003. Autophagy genes are essential for dauer development and life-span extension in C. elegans. *Science,* 301**,** 1387-91.

MIZUSHIMA, N. & KOMATSU, M. 2011. Autophagy: renovation of cells and tissues. *Cell,* 147**,** 728-41.

MIZUSHIMA, N., LEVINE, B., CUERVO, A. M. & KLIONSKY, D. J. 2008. Autophagy fights disease through cellular self-digestion. *Nature,* 451**,** 1069-75.

MOORE, B. T., JORDAN, J. M. & BAUGH, L. R. 2013. WormSizer: high-throughput analysis of nematode size and shape. *PLoS One,* 8**,** e57142.

MOREIN, S., ANDERSSON, A., RILFORS, L. & LINDBLOM, G. 1996. Wild-type Escherichia coli cells regulate the membrane lipid composition in a "window" between gel and non-lamellar structures. *J Biol Chem,* 271**,** 6801-9.

MOTA, M., BANINI, B. A., CAZANAVE, S. C. & SANYAL, A. J. 2016. Molecular mechanisms of lipotoxicity and glucotoxicity in nonalcoholic fatty liver disease. *Metabolism,* 65**,** 1049-61.

NG, B. S. H., SHYU, P. T., CHAW, R., SEAH, Y. L. & THIBAULT, G. 2017. Lipid perturbation compromises UPR-mediated ER homeostasis as a result of premature degradation of membrane proteins. *bioRxiv*.

NG, D. T., SPEAR, E. D. & WALTER, P. 2000. The unfolded protein response regulates multiple aspects of secretory and membrane protein biogenesis and endoplasmic reticulum quality control. *J Cell Biol,* 150**,** 77-88.

NOVOA, I., ZENG, H., HARDING, H. P. & RON, D. 2001. Feedback inhibition of the unfolded protein response by GADD34-mediated dephosphorylation of eIF2alpha. *J Cell Biol,* 153**,** 1011-22.

OGATA, M., HINO, S., SAITO, A., MORIKAWA, K., KONDO, S., KANEMOTO, S., MURAKAMI, T., TANIGUCHI, M., TANII, I., YOSHINAGA, K., SHIOSAKA, S., HAMMARBACK, J. A., URANO, F. & IMAIZUMI, K. 2006. Autophagy is activated for cell survival after endoplasmic reticulum stress. *Mol Cell Biol,* 26**,** 9220-31.

OGG, S. & RUVKUN, G. 1998. The C. elegans PTEN homolog, DAF-18, acts in the insulin receptor-like metabolic signaling pathway. *Mol Cell,* 2**,** 887-93.

OURSEL, D., LOUTELIER-BOURHIS, C., ORANGE, N., CHEVALIER, S., NORRIS, V. & LANGE, C. M. 2007. Lipid composition of membranes of Escherichia coli by liquid chromatography/tandem mass spectrometry using negative electrospray ionization. *Rapid Commun Mass Spectrom,* 21**,** 1721-8.

OYADOMARI, S., KOIZUMI, A., TAKEDA, K., GOTOH, T., AKIRA, S., ARAKI, E. & MORI, M. 2002. Targeted disruption of the Chop gene delays endoplasmic reticulum stress-mediated diabetes. *J Clin Invest,* 109**,** 525-32.

OZCAN, U., CAO, Q., YILMAZ, E., LEE, A. H., IWAKOSHI, N. N., OZDELEN, E., TUNCMAN, G., GORGUN, C., GLIMCHER, L. H. & HOTAMISLIGIL, G. S. 2004. Endoplasmic reticulum stress links obesity, insulin action, and type 2 diabetes. *Science,* 306**,** 457-61.

PALAVALLI, L. H., BRENDZA, K. M., HAAKENSON, W., CAHOON, R. E., MCLAIRD, M., HICKS, L. M., MCCARTER, J. P., WILLIAMS, D. J., HRESKO, M. C. & JEZ, J. M. 2006. Defining the role of phosphomethylethanolamine N-methyltransferase from Caenorhabditis elegans in phosphocholine biosynthesis by biochemical and kinetic analysis. *Biochemistry,* 45**,** 6056-65.

PATTINGRE, S., BAUVY, C., CARPENTIER, S., LEVADE, T., LEVINE, B. & CODOGNO, P. 2009. Role of JNK1-dependent Bcl-2 phosphorylation in ceramide-induced macroautophagy. *J Biol Chem,* 284**,** 2719-28.

PROMLEK, T., ISHIWATA-KIMATA, Y., SHIDO, M., SAKURAMOTO, M., KOHNO, K. & KIMATA, Y. 2011. Membrane aberrancy and unfolded proteins activate the endoplasmic reticulum stress sensor Ire1 in different ways. *Mol Biol Cell,* 22**,** 3520-32.

PURI, P., BAILLIE, R. A., WIEST, M. M., MIRSHAHI, F., CHOUDHURY, J., CHEUNG, O., SARGEANT, C., CONTOS, M. J. & SANYAL, A. J. 2007. A lipidomic analysis of nonalcoholic fatty liver disease. *Hepatology,* 46**,** 1081-90.

RINELLA, M. E. & SANYAL, A. J. 2015. NAFLD in 2014: Genetics, diagnostics and therapeutic advances in NAFLD. *Nat Rev Gastroenterol Hepatol,* 12**,** 65-6.

RUBIO, C., PINCUS, D., KORENNYKH, A., SCHUCK, S., EL-SAMAD, H. & WALTER, P. 2011. Homeostatic adaptation to endoplasmic reticulum stress depends on Ire1 kinase activity. *J Cell Biol,* 193**,** 171-84.

RUTKOWSKI, D. T., ARNOLD, S. M., MILLER, C. N., WU, J., LI, J., GUNNISON, K. M., MORI, K., SADIGHI AKHA, A. A., RADEN, D. & KAUFMAN, R. J. 2006. Adaptation to ER stress is mediated by differential stabilities of pro-survival and pro-apoptotic mRNAs and proteins. *PLoS Biol,* 4**,** e374.

SCHRODER, M. & KAUFMAN, R. J. 2005. ER stress and the unfolded protein response. *Mutat Res,* 569**,** 29-63.

SENFT, D. & RONAI, Z. A. 2015. UPR, autophagy, and mitochondria crosstalk underlies the ER stress response. *Trends Biochem Sci,* 40**,** 141-8.

SHEN, X., ELLIS, R. E., SAKAKI, K. & KAUFMAN, R. J. 2005. Genetic interactions due to constitutive and inducible gene regulation mediated by the unfolded protein response in C. elegans. *PLoS Genet,* 1**,** e37.

SHEN, X., ZHANG, K. & KAUFMAN, R. J. 2004. The unfolded protein response--a stress signaling pathway of the endoplasmic reticulum. *J Chem Neuroanat,* 28**,** 79-92.

SINGH, R., KAUSHIK, S., WANG, Y., XIANG, Y., NOVAK, I., KOMATSU, M., TANAKA, K., CUERVO, A. M. & CZAJA, M. J. 2009. Autophagy regulates lipid metabolism. *Nature,* 458**,** 1131-5.

SMULAN, L. J., DING, W., FREINKMAN, E., GUJJA, S., EDWARDS, Y. J. K. & WALKER, A. K. 2016. Cholesterol-Independent SREBP-1 Maturation Is Linked to ARF1 Inactivation. *Cell Rep,* 16**,** 9-18.

SO, J. S., HUR, K. Y., TARRIO, M., RUDA, V., FRANK-KAMENETSKY, M., FITZGERALD, K., KOTELIANSKY, V., LICHTMAN, A. H., IWAWAKI, T., GLIMCHER, L. H. & LEE, A. H. 2012. Silencing of lipid metabolism genes through IRE1alpha-mediated mRNA decay lowers plasma lipids in mice. *Cell Metab,* 16**,** 487-99.

SRIBURI, R., JACKOWSKI, S., MORI, K. & BREWER, J. W. 2004. XBP1: a link between the unfolded protein response, lipid biosynthesis, and biogenesis of the endoplasmic reticulum. *J Cell Biol,* 167**,** 35-41.

STIERNAGLE, T. 2006. Maintenance of C. elegans. *WormBook***,** 1-11.

SUPEK, F., BOSNJAK, M., SKUNCA, N. & SMUC, T. 2011. REVIGO summarizes and visualizes long lists of gene ontology terms. *PLoS One,* 6**,** e21800.

TAKACS-VELLAI, K., VELLAI, T., PUOTI, A., PASSANNANTE, M., WICKY, C., STREIT, A., KOVACS, A. L. & MULLER, F. 2005. Inactivation of the autophagy gene bec-1 triggers apoptotic cell death in C. elegans. *Curr Biol,* 15**,** 1513-7.

TALLOCZY, Z., JIANG, W., VIRGIN, H. W. T., LEIB, D. A., SCHEUNER, D., KAUFMAN, R. J., ESKELINEN, E. L. & LEVINE, B. 2002. Regulation of starvation- and virus-induced autophagy by the eIF2alpha kinase signaling pathway. *Proc Natl Acad Sci U S A,* 99**,** 190-5.

TAM, A. B., ROBERTS, L. S., CHANDRA, V., RIVERA, I. G., NOMURA, D. K., FORBES, D. J. & NIWA, M. 2018. The UPR Activator ATF6 Responds to Proteotoxic and Lipotoxic Stress by Distinct Mechanisms. *Dev Cell,* 46**,** 327-343 e7.

THIBAULT, G., ISMAIL, N. & NG, D. T. 2011. The unfolded protein response supports cellular robustness as a broad-spectrum compensatory pathway. *Proc Natl Acad Sci U S A,* 108**,** 20597-602.

THIBAULT, G., SHUI, G., KIM, W., MCALISTER, G. C., ISMAIL, N., GYGI, S. P., WENK, M. R. & NG, D. T. 2012. The membrane stress response buffers lethal effects of lipid disequilibrium by reprogramming the protein homeostasis network. *Mol Cell,* 48**,** 16-27.

TIAN, Y., LI, Z., HU, W., REN, H., TIAN, E., ZHAO, Y., LU, Q., HUANG, X., YANG, P., LI, X., WANG, X., KOVACS, A. L., YU, L. & ZHANG, H. 2010. C. elegans screen identifies autophagy genes specific to multicellular organisms. *Cell,* 141**,** 1042-55.

TIMMONS, L. & FIRE, A. 1998. Specific interference by ingested dsRNA. *Nature,* 395**,** 854.

TINIAKOS, D. G., VOS, M. B. & BRUNT, E. M. 2010. Nonalcoholic fatty liver disease: pathology and pathogenesis. *Annu Rev Pathol,* 5**,** 145-71.

TRAVERS, K. J., PATIL, C. K., WODICKA, L., LOCKHART, D. J., WEISSMAN, J. S. & WALTER, P. 2000. Functional and genomic analyses reveal an essential coordination between the unfolded protein response and ER-associated degradation. *Cell,* 101**,** 249-58.

URANO, F., CALFON, M., YONEDA, T., YUN, C., KIRALY, M., CLARK, S. G. & RON, D. 2002. A survival pathway for Caenorhabditis elegans with a blocked unfolded protein response. *J Cell Biol,* 158**,** 639-46.

VIDAL, R. L., FIGUEROA, A., COURT, F. A., THIELEN, P., MOLINA, C., WIRTH, C., CABALLERO, B., KIFFIN, R., SEGURA-AGUILAR, J., CUERVO, A. M., GLIMCHER, L. H. & HETZ, C. 2012. Targeting the UPR transcription factor XBP1 protects against Huntington's disease through the regulation of FoxO1 and autophagy. *Hum Mol Genet,* 21**,** 2245-62.

VOLMER, R. & RON, D. 2015. Lipid-dependent regulation of the unfolded protein response. *Curr Opin Cell Biol,* 33**,** 67-73.

VOLMER, R., VAN DER PLOEG, K. & RON, D. 2013. Membrane lipid saturation activates endoplasmic reticulum unfolded protein response transducers through their transmembrane domains. *Proc Natl Acad Sci U S A,* 110**,** 4628-33.

WALKER, A. K., JACOBS, R. L., WATTS, J. L., ROTTIERS, V., JIANG, K., FINNEGAN, D. M., SHIODA, T., HANSEN, M., YANG, F., NIEBERGALL, L. J., VANCE, D. E., TZONEVA, M., HART, A. C. & NAAR, A. M. 2011. A conserved SREBP-1/phosphatidylcholine feedback circuit regulates lipogenesis in metazoans. *Cell,* 147**,** 840-52.

WALKEY, C. J., YU, L., AGELLON, L. B. & VANCE, D. E. 1998. Biochemical and evolutionary significance of phospholipid methylation. *J Biol Chem,* 273**,** 27043-6.

WALTER, P. & RON, D. 2011. The unfolded protein response: from stress pathway to homeostatic regulation. *Science,* 334**,** 1081-6.

WANG, C., SAAR, V., LEUNG, K. L., CHEN, L. & WONG, G. 2018. Human amyloid beta peptide and tau co-expression impairs behavior and causes specific gene expression changes in Caenorhabditis elegans. *Neurobiol Dis,* 109**,** 88-101.

WANG, S., CHEN, Z., LAM, V., HAN, J., HASSLER, J., FINCK, B. N., DAVIDSON, N. O. & KAUFMAN, R. J. 2012. IRE1alpha-XBP1s induces PDI expression to increase MTP activity for hepatic VLDL assembly and lipid homeostasis. *Cell Metab,* 16**,** 473-86.

WEI, Y., PATTINGRE, S., SINHA, S., BASSIK, M. & LEVINE, B. 2008a. JNK1-mediated phosphorylation of Bcl-2 regulates starvation-induced autophagy. *Mol Cell,* 30**,** 678-88.

WEI, Y., SINHA, S. & LEVINE, B. 2008b. Dual role of JNK1-mediated phosphorylation of Bcl-2 in autophagy and apoptosis regulation. *Autophagy,* 4**,** 949-51.

WILLY, J. A., YOUNG, S. K., STEVENS, J. L., MASUOKA, H. C. & WEK, R. C. 2015. CHOP links endoplasmic reticulum stress to NF-kappaB activation in the pathogenesis of nonalcoholic steatohepatitis. *Mol Biol Cell,* 26**,** 2190-204.

WU, H., NG, B. S. & THIBAULT, G. 2014. Endoplasmic reticulum stress response in yeast and humans. *Biosci Rep,* 34.

YAMAMOTO, K., TAKAHARA, K., OYADOMARI, S., OKADA, T., SATO, T., HARADA, A. & MORI, K. 2010. Induction of liver steatosis and lipid droplet formation in ATF6alpha-knockout mice burdened with pharmacological endoplasmic reticulum stress. *Mol Biol Cell,* 21**,** 2975-86.

YOUNCE, C. & KOLATTUKUDY, P. 2012. MCP-1 induced protein promotes adipogenesis via oxidative stress, endoplasmic reticulum stress and autophagy. *Cell Physiol Biochem,* 30**,** 307-20.

ZHAO, Y., LI, X., CAI, M. Y., MA, K., YANG, J., ZHOU, J., FU, W., WEI, F. Z., WANG, L., XIE, D. & ZHU, W. G. 2013. XBP-1u suppresses autophagy by promoting the degradation of FoxO1 in cancer cells. *Cell Res,* 23**,** 491-507.

Figures

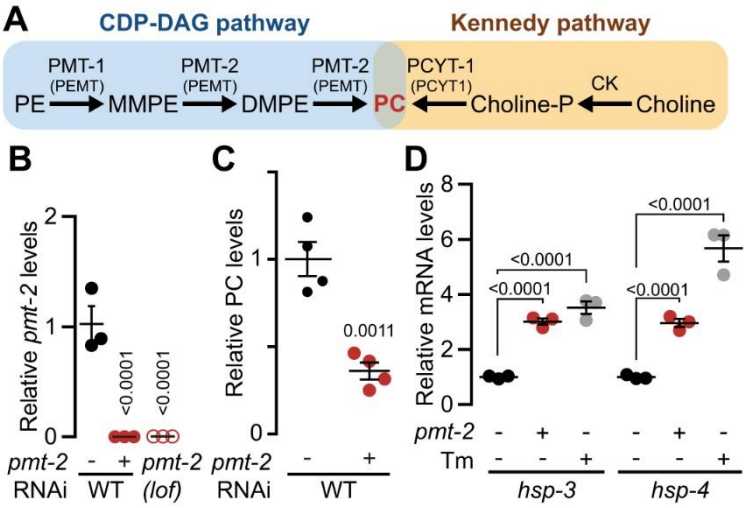

Figure 1. *pmt-2* silencing is sufficient to activate the UPR by lipid bilayer stress.

(A) Metabolic pathways for the synthesis of phosphatidylcholine in *C. elegans*. Human orthologues are highlighted in brackets. PE, phosphatidylethanolamine; MMPE, monomethyl-phosphatidylethanolamine; DMPE, dimethyl-phosphatidylethanolamine; PMT-1/2, phosphatidylethanolamine N-methyltransferase 1/2; PEMT, phosphatidylethanolamine N-methyltransferase; PCYT-1, choline-phosphate cytidylyltransferase 1; CK, choline kinase. (B) qPCR results comparing expression of *pmt-2* in *pmt-2(RNAi)* and in *pmt-2(lof)* animals (C) Comparison of PC levels in WT and *pmt-2(RNAi)* animals by GC-FID. (D) qPCR results comparing the expression of UPR marker genes *hsp-3* and *hsp-4* in *pmt-2(RNAi)* and WT worms treated with 25 µg/ml tunicamycin for 4 h. Data shown is the mean ± s.e.m. of at least three independent experiments. Statistical analysis was subjected to one-way ANOVA followed by Tukey's multiple comparisons adjustment (B,D) or two-tailed Student's t-test (C). ns, non-significant.

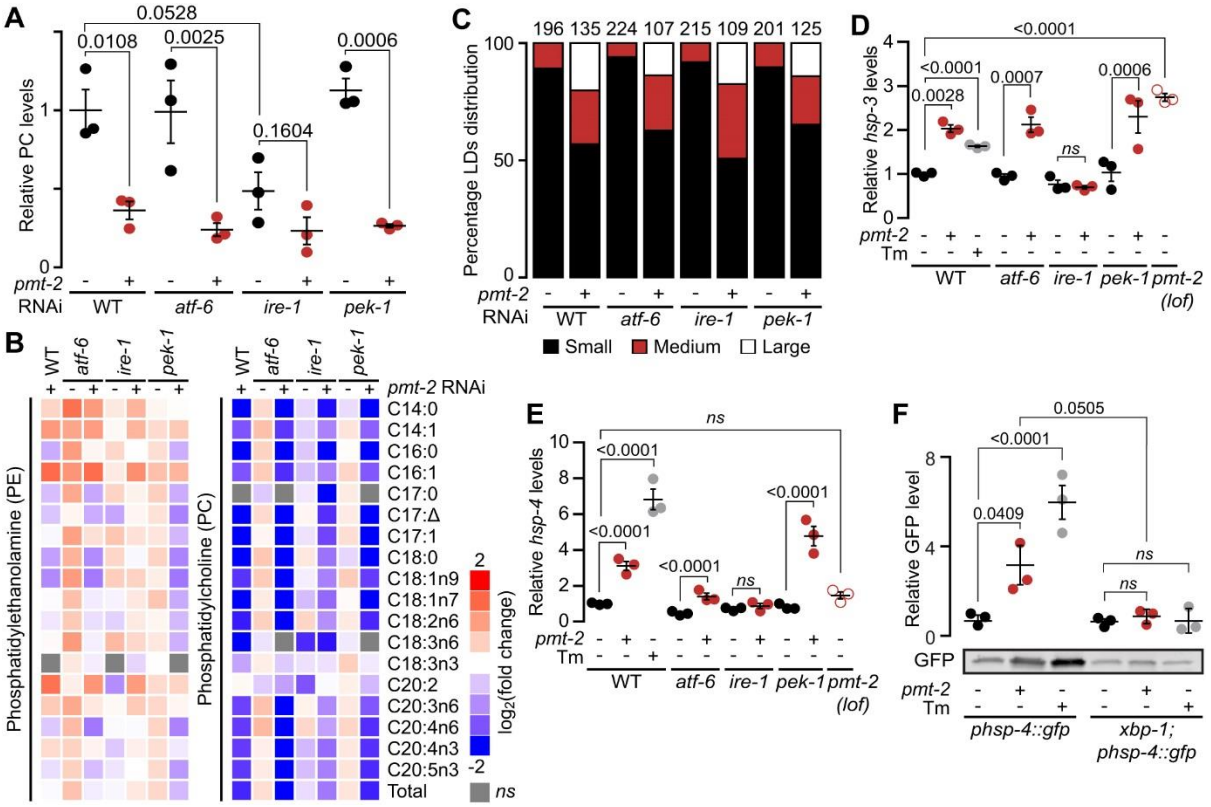

Figure 2. UPR^{LBS} leads to the accumulation of lipid droplets.

(A) Comparison of PC levels in WT, *atf-6(lof)*, *ire-1(lof)* and *pek-1(lof)* animals treated with *pmt-2* RNAi as quantified by GC-FID. (B) Heat map representation of all significant PE- and PC-derived fatty acids changes to untreated WT. WT and mutant worms were treated as in **A**. (C) Lipid droplet (LD) size distribution quantified from bright field images of Sudan Black B staining of WT and mutant animals treated as in **A**. LD sizes are classified into small (0.8 – 3 μM), medium (3.1 – 6 μM) and large (>6 μM) categories. Numbers above each bar refer to lipid droplets present per worm. WT, n=12 (-), n=15 (+); *atf-6(lof)*, n=13 (-), n=14 (+); *ire-1(lof)*, n=18 (-), n=14 (+); *pek-1(lof)*, n=12 (-), n=13 (+), respectively. Representative images are shown in Fig S3A. (D, E) qPCR results comparing the expression of UPR marker genes *hsp-3* and *hsp-4* in WT and mutant animals treated as in **A** and WT worms treated 4 h with 25 μg/ml tunicamycin. (F) Quantification of immunoblot signalling of worms treated as in **A** with anti-GFP antibodies and normalized to REVERT Total Protein Stain (Representative blot is shown in Fig. S3B). Data shown is the mean ± s.e.m. of at least three independent experiments. Statistical analysis was subjected to one-way ANOVA followed by Tukey's multiple comparisons adjustment. ns, non-significant.

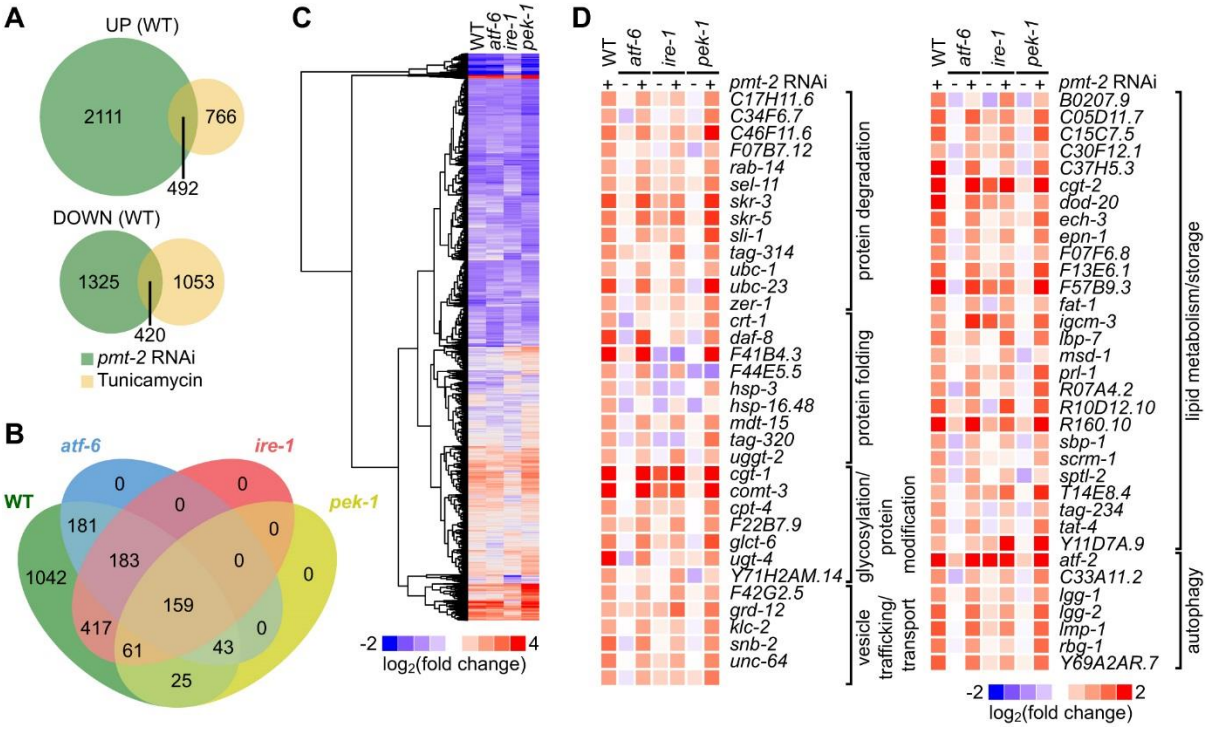

Figure 3. UPR^{LBS} and UPR^{PT} lead to distinct transcriptomic outcomes.

(A) Venn diagram representation of upregulated (UP) and downregulated (DOWN) genes at a minimum of 1.5-fold in *pmt-2(RNAi)* and WT worms treated with 25 µg/ml tunicamycin for 4 h compared to untreated WT worms. (B) Four-way Venn diagram depicts transcriptional targets of WT, *atf-6(lof), ire-1(lof)* and *pek-1(lof)* worms upregulated during lipid bilayer stress and excluding genes commonly upregulated from *pmt-2* RNAi and tunicamycin treatments. Fold-change > 1.5, ANOVA *P* values < 0.05. (C) Hierarchical clustering of 8045 genes with significant changes based on Pearson correlation coefficients. Gene expression of WT, *atf-6(lof), ire-1(lof), pek-1(lof)* worms treated with *pmt-2* RNAi were compared against their respective untreated worms (empty vector). (D) Heat map representation of previously reported UPR-regulated genes of worms derived from **C**. Gene expression $\log_2$ fold changes were normalized to untreated WT worms.

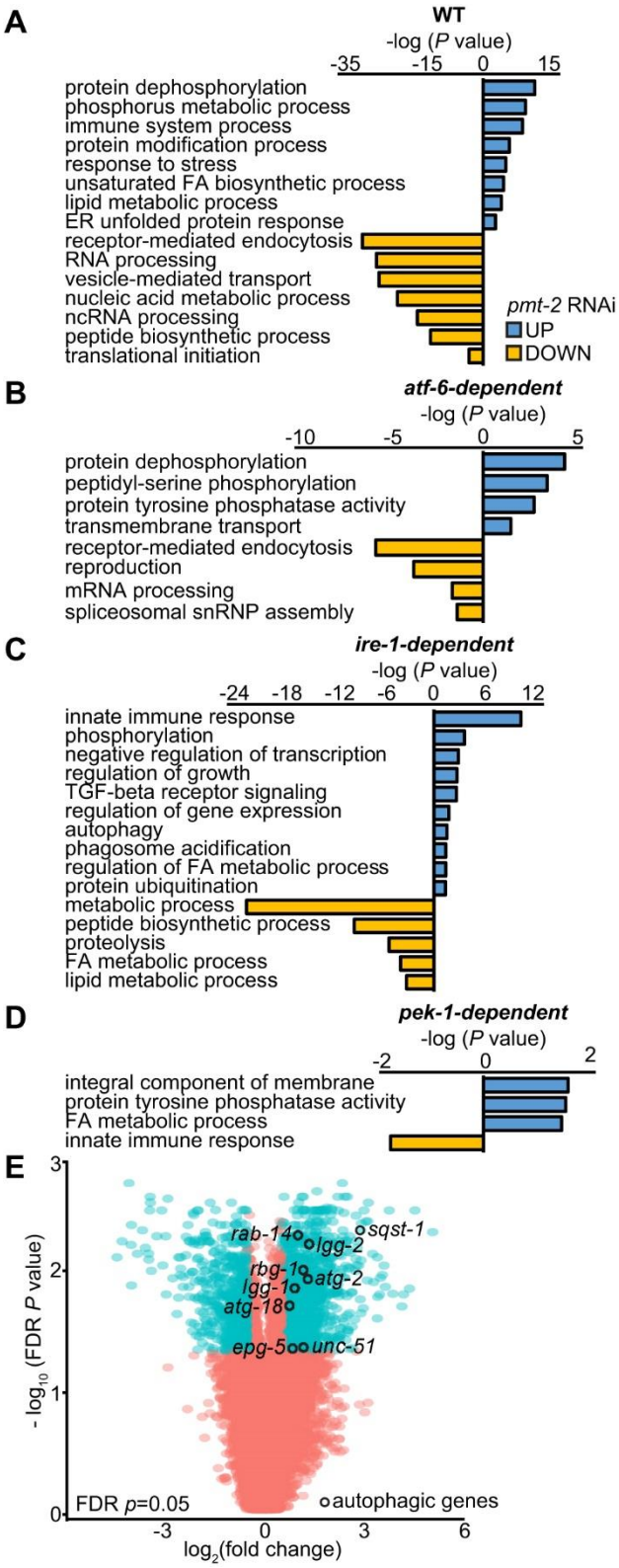

Figure 4. Depletion of PC increases autophagy and lipid metabolism activity in an IRE-1-dependent manner.

(A-D) Bar plot of the GO analysis of genes upregulated (blue) and downregulated (yellow) in WT (A), *atf-6(lof)* (B), *ire-1(lof)* (C) and *pek-1(lof)* (D) subjected to *pmt-2* RNAi and compared to their respective untreated strains (empty vector). Genes are highlighted in yellow in Table S5. (E) Volcano plot depicting changes in gene expression during UPR^{LBS}. Log_2 gene fold changes are plotted against negative log_{10} FDR p values. Genes that are upregulated or downregulated by more than 1.5-fold and with false-discovery rate (FDR) < 0.05 are labelled in black circles. Autophagic (opened circle) genes regulated in an IRE-1-dependent manner are shown in black.

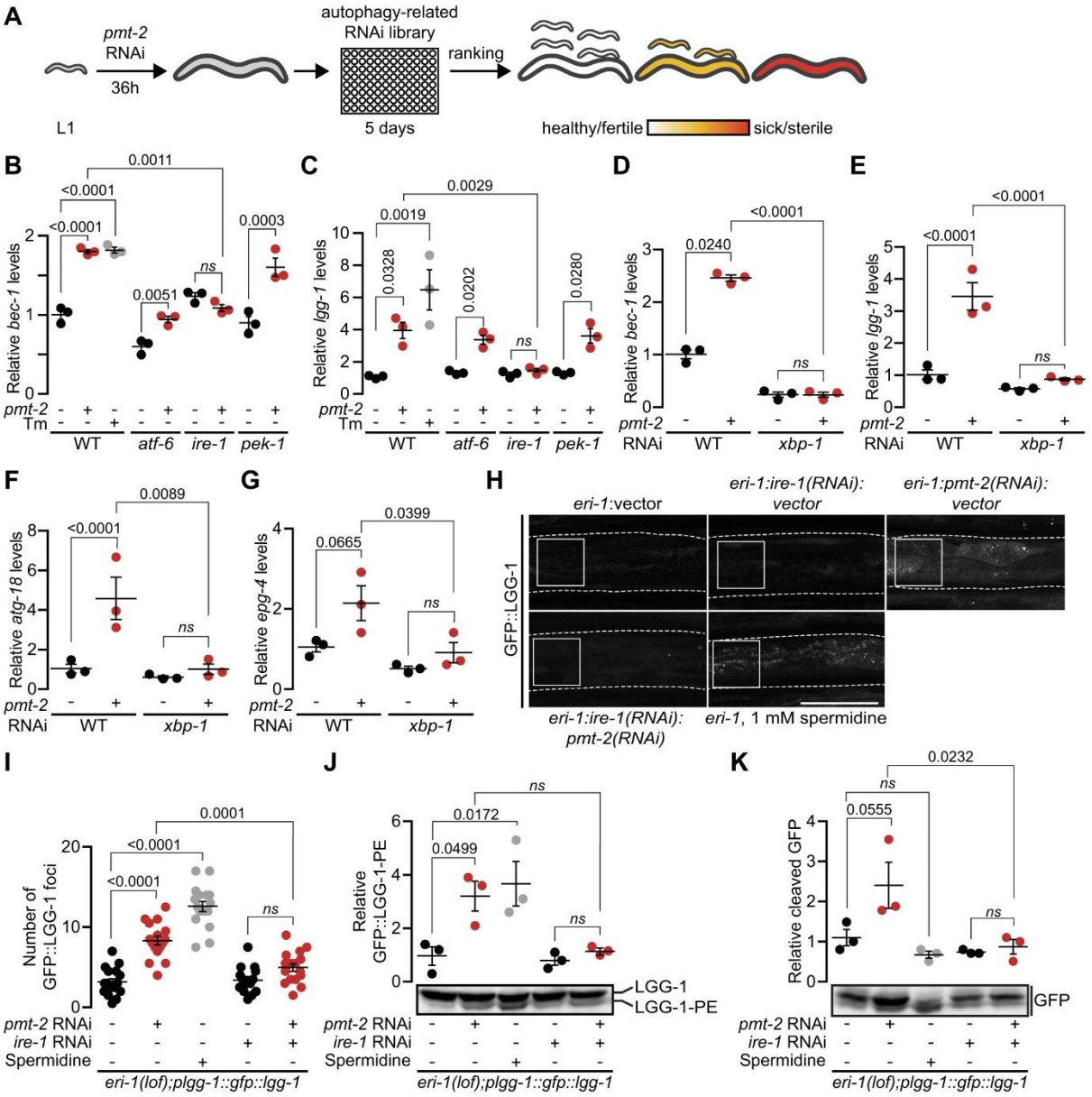

Figure 5. A subset of autophagy genes is regulated through the IRE-1/XBP-1 axis upon lipid bilayer stress-induced UPR.

(A) Schematic representation of the RNAi screening to identify potential autophagy genes that participate in lipid bilayer stress. WT worms were treated with *pmt-2* RNAi for 36 h and subsequently transferred to 96-well plates containing RNAi of autophagy-related target genes. Worms were scored for growth defects, sterility, mobility and embryonic lethality. qPCR comparing expression of *bec-1* (B) and *lgg-1* (C) in WT, *atf-6(lof), ire-1(lof)* and *pek-1(lof)* worms. qPCR comparing expression of *bec-1* (D), *lgg-1* (E), *atg-18* (F), and *epg-4* (G) in WT and *xbp-1(lof)* animals treated with *pmt-2* RNAi. Representative fluorescence images (H) and quantification of GFP::LGG-1 puncta (I) in the anterior intestines of *eri-1;plgg-1::gfp::lgg-1* worms treated for 48 h with *pmt-2* RNAi, *ire-1* RNAi, 1 mM spermidine or a combination of *ire-1* and *pmt-2* RNAis. Solid box depicts quantification area, dashed lines show the outline of worms. Scale bar, 50 µm. n=17, n=16, n=17, n=15, n=18, for *eri-1*:vector, *eri-*

1:pmt-2(RNAi), *eri-1* treated with 1 mM spermidine, *eri-1:ire-1(RNAi)*, *eri-1*:*ire-1(RNAi):pmt-2(RNAi),* respectively. Separation of GFP::LGG-1-PE (J) and cleaved GFP (K) in *eri-1;plgg-1::gfp::lgg-1* worm lysate treated as in **H** and **I**. The lysates were prepared and analysed by immunoblotting with anti-GFP antibodies and normalized to total protein loading control (Fig. S6H). Cleaved GFP represents autophagic flux where the GFP degradation takes place at the autolysosomes. As a measure of autophagic flux, ratios of GFP::LGG-1-PE to total protein and of cleaved GFP to total proteins were compared. Data shown is the mean ± s.e.m. of at least three independent experiments. Statistical analysis was subjected to one-way ANOVA followed by Tukey's multiple comparisons adjustment. ns, non-significant.

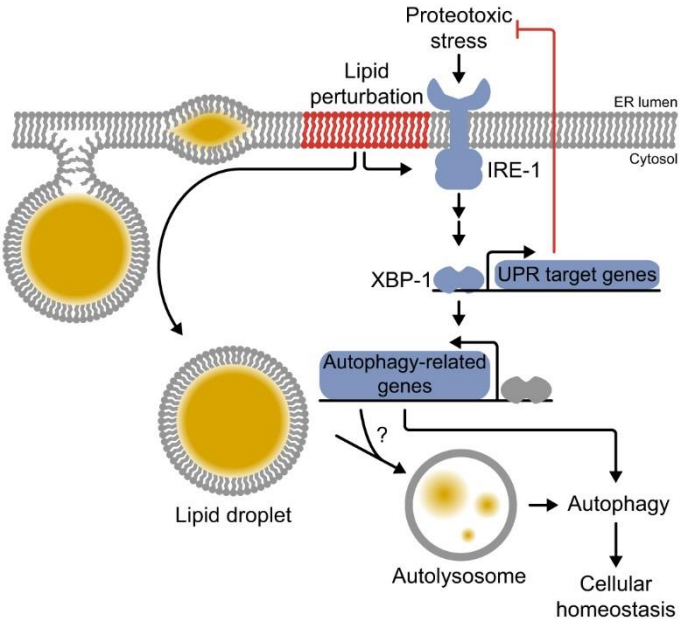

Figure 6. UPR^{LBS} regulates autophagy through the canonical IRE-1/XBP-1 UPR branch.
Proteotoxic-induced ER stress activates a subset of UPR target genes to restore ER homeostasis. In addition, lipid bilayer stress-induced ER stress partially induces autophagy through the IRE-1/XBP-1 axis. Intact of autophagy function during proteotoxic or lipid bilayer stress is essential in maintaining cellular homeostasis and contributes to organismal health span.

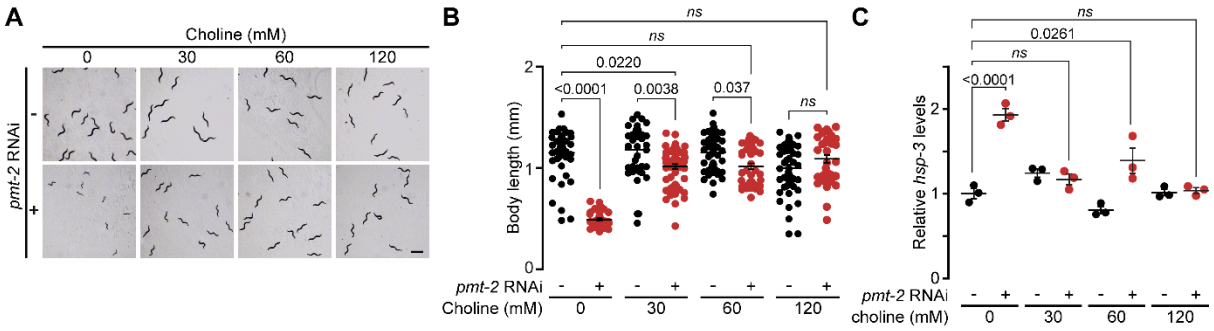

Figure S1, Refers to **Figure 1**. **Choline supplementation restores developmental defects in *pmt-2(RNAi)* animals.**
(A) Representative choline rescue assay of *pmt-2(RNAi)* developmental defect. L1 worms were grown on *pmt-2* RNAi or empty vector on plates supplemented with 0, 30, 60, or 120 mM choline, and images were taken after 48 h. Scale bar, 100 µm. (B) Body length quantification of worms from **A**. WT, 0 mM choline, n=47(-), n=32(+); 30 mM choline, n=39(-), n=58(+); 60 mM choline, n=48(-), n=43(+); 120 mM choline, n=54(-), n=38(+). (C) qPCR of *hsp-3* expression level in WT worms treated as in **A**. Data shown is the mean ± s.e.m. of at least three independent experiments. Statistical analysis was subjected to one-way ANOVA followed by Tukey's multiple comparisons adjustment. ns, non-significant.

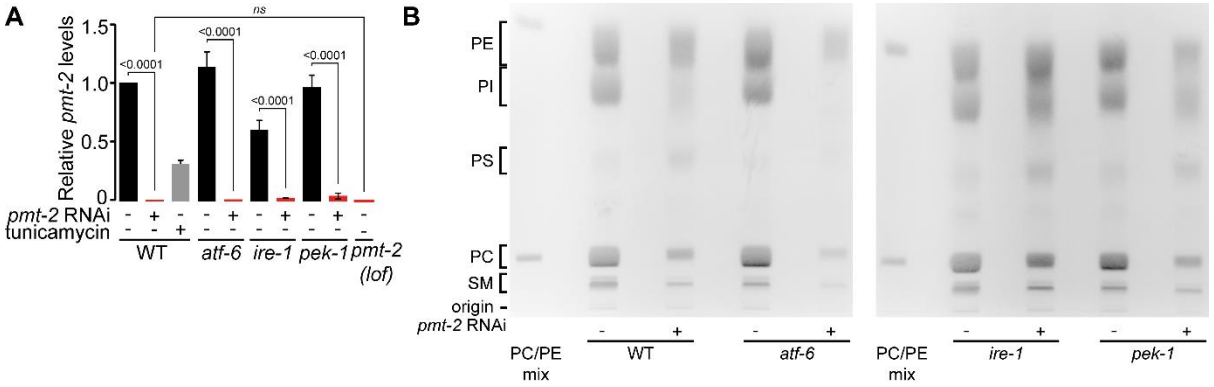

Figure S2, Refers to **Figure 2A-B**. **Inactivation of *pmt-2* decreased PC content in worms.**
(A) qPCR of *pmt-2* expression after *pmt-2* RNAi treatment in WT, *atf-6(lof)*, *ire-1(lof),* and *pek-1(lof)* worms. *pmt-2(lof)* worms were used as a control. *pmt-2* RNAi treatment efficiently silenced expression of *pmt-2* across all the strains tested. (B) Representative separation of PE, MMPE, DMPE, and PC from total lipid extract using thin-layer chromatography (TLC). Comparison of phospholipid levels in WT, *atf-6(lof)*, *ire-1(lof)* and *pek-1(lof)* animals treated with *pmt-2* RNAi. POPE (1-palmitoyl-2-oleoyl-sn-glycero-3-phosphoethanolamine; 16:0-18:1n9 PE) and DOPC (1,2-dioleoyl-sn-glycero-3-phosphocholine; 18:1n9 PC) were used as markers. Data shown is the mean ± s.e.m. of at least three independent experiments. Statistical analysis was subjected to one-way ANOVA followed by Tukey's multiple comparisons adjustment. ns, non-significant.

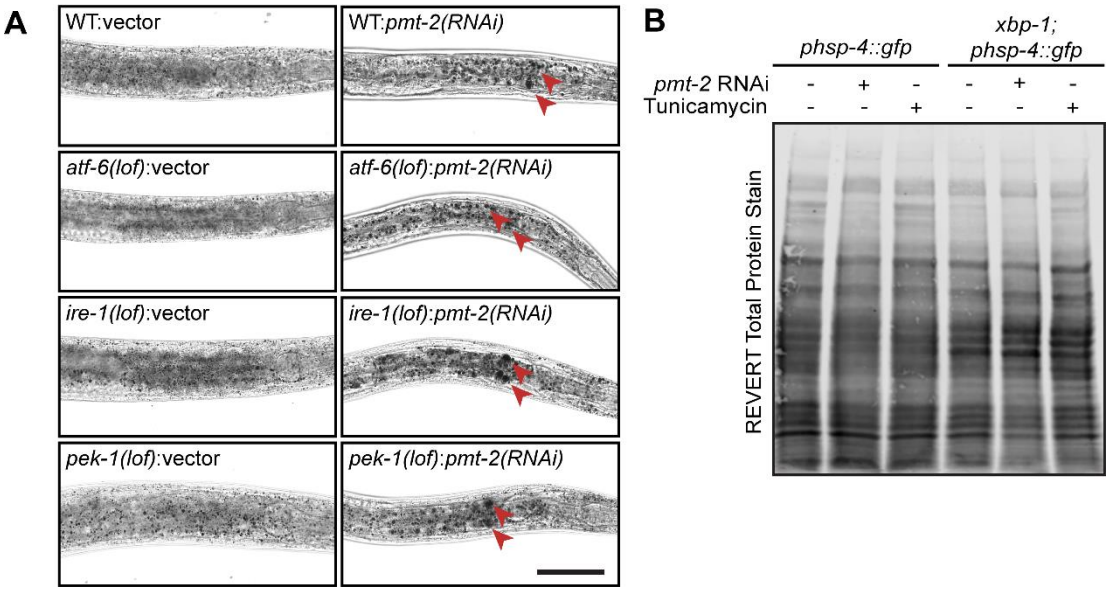

Figure S3, Refers to **Figure 2C,F**. **Lipid perturbation induces lipid droplets accumulation and activates the UPR.**
(A) Representative images of lipid droplet visualised using Sudan Black B staining of WT, *atf-6(lof)*, *ire-1(lof)* and *pek-1(lof)* animals treated with *pmt-2* RNAi. Brightfield images of stained worms are shown using 63X objective lens. Red arrowhead highlights large LDs. Scale bar, 100 µm. (B) Total protein stain verified equal loading and served as normalization control for the immunoblot.

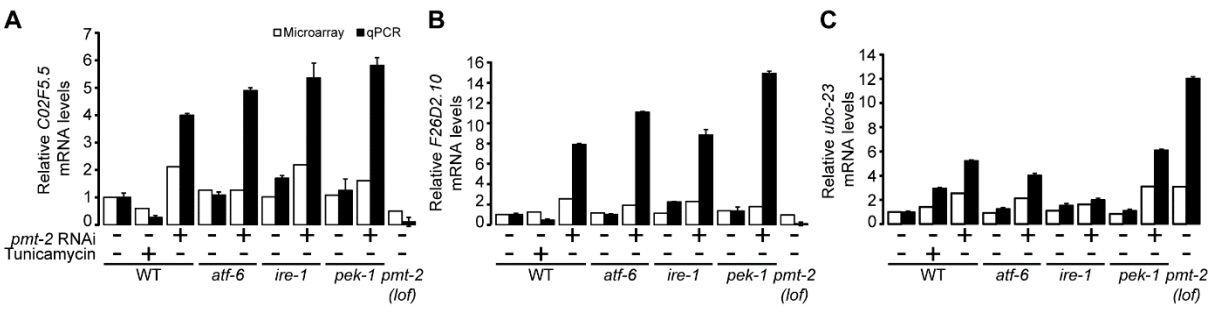

Figure S4, Refers to **Figure 3**. **Validation of DNA microarray analysis using quantitative real-time PCR.**
(A-C) Comparison of *C02F5.5* (A), *F26D2.10* (B), and *ubc-23* (C) gene expression in WT, *atf-6(lof)*, *ire-1(lof)* and *pek-1(lof)* animals treated with *pmt-2* RNAi by DNA microarray (white bars) and qPCR (black bars). *C02F5.5* and *F26D2.10*, are both uncharacterized genes; *ubc-23*, a member of the BCL-2 family. The figure represents technical triplicates.

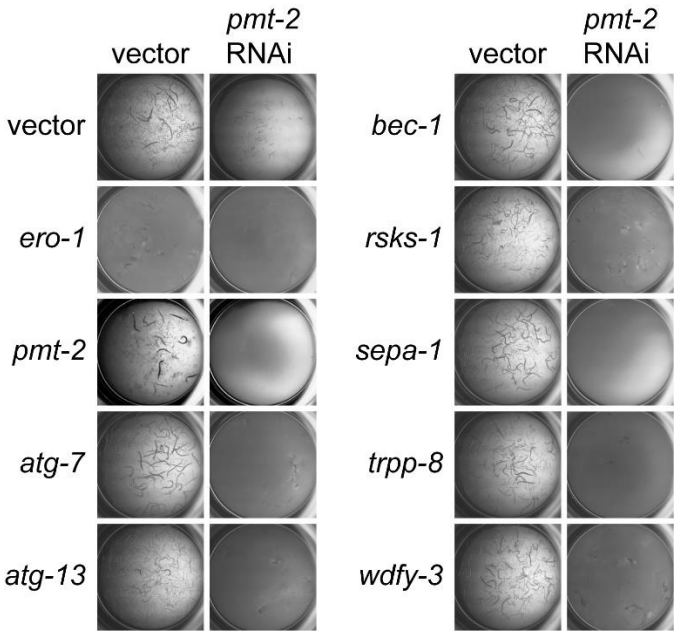

Figure S5, Refers to Figure 5. **Autophagy is essential during lipid perturbation.** WT worms were treated with vector or *pmt-2* RNAi for 36 h and subsequently subjected to RNAi in liquid media in a 96-well plate for 5 days. The worms were scored based on their developmental defects as described in Fig. 5A. *ero-1* RNAi was included as a positive control.

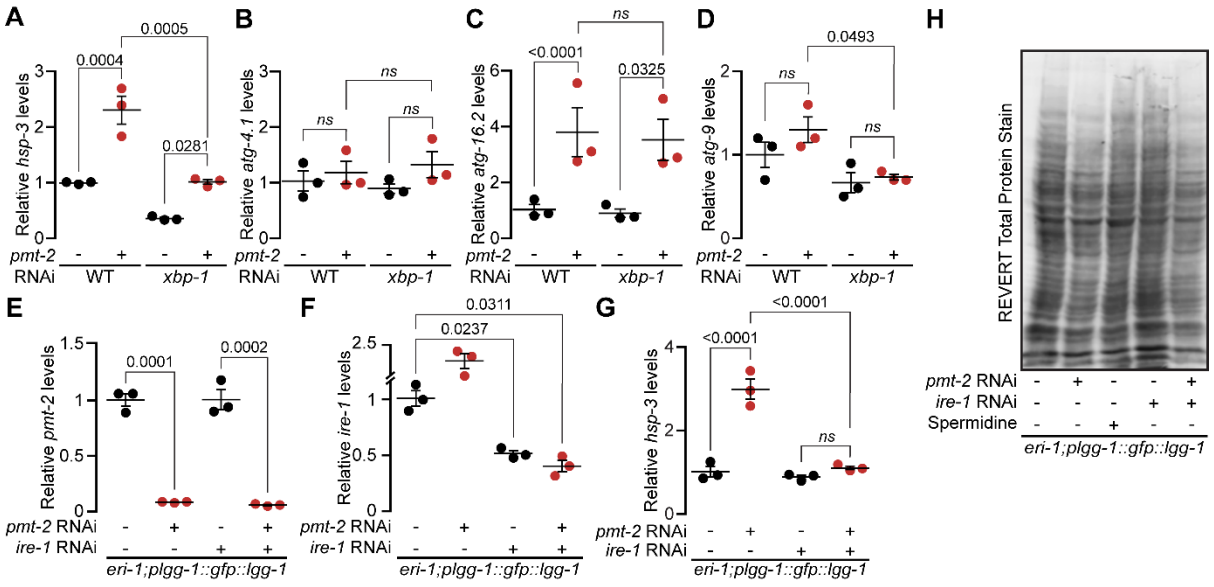

Figure S6, Refers to Figure 5. **Autophagy is partially dependent on XBP-1**. qPCR comparing expression of *hsp-3* (A), *atg-4.1* (B), *atg-16.2* (C), *atg-9* (D) in WT and *xbp-1(lof)* mutants treated with *pmt-2* RNAi. qPCR comparing expression of *pmt-2* (E), *ire-1* (F), *hsp-3* (G) in *eri-1;plgg-1::gfp::lgg-1* worms treated with *pmt-2, ire-1*, and *ire-1:pmt-2* RNAis; technical triplicates. (H) Total protein stain verified equal loading and served as normalization control for the immunoblot. Data shown is the mean ± s.e.m. of at least three independent experiments. Statistical analysis was subjected to one-way ANOVA followed by Tukey's multiple comparisons adjustment. ns, non-significant.

Table S1. Oligonucleotide primers used in the study.

Gene	Sequence (5' to 3')	Assay
act-1	AGGACTGGGTGCTCTTCTGG GAGCACGGTATCGTCACCAA	qPCR
atg-4.1	AGGAAGATGGAATCGAGGCAA TGCAACCCCATCCTTGATCC	qPCR
atg-9	ATGGAATCGTTCTTCTCACTG GCAGGAGGTATTGTATCTTCTC	qPCR
atg-16.2	ATGTGCTGGCTGGATCTTCG GAGCCGAATCTGATCTCGCAG	qPCR
atg-18	CCGAAGTCAGACACTAGTCGAG TCGGAACCGATTGGTTGCTTG	qPCR
bec-1	AAGCTCTGACTGGACATTCTCG GCGTCAGAGCAATCATTACAAAC	qPCR
atg-18	CCGAAGTCAGACACTAGTCGAG TCGGAACCGATTGGTTGCTTG	qPCR
C02F5.5	CATCTTTTGAGCTTATGATGGTGCT AAGCACCAAGGAACACGAGAT	qPCR
epg-4	CCAATTCCTCTTATCACACCA GTCGAAGAAGTAATCGAAACAG	qPCR
F26D2.10	CTCTTGTGGCAGCTCATGGT CGTGGATCAAAAACAGCGGC	qPCR
hsp-3	AGAAGGAGACCAAGTATGGAACC TGATACGGTTTCCTTGGTCGTT	qPCR
hsp-4	CATCTCGTGGAATCAACCCT TGACGTCAAGAAGGACAACA	qPCR
lgg-1	TCGTGATGGTCCTGGTAGAGT ACGCATCCAACTTCGTCCA	qPCR
ire-1	ACAATGGCTAGTCAGCGAGG CAATCCAGCCATCGGTTCCT	qPCR
pmt-2	AGAACGTGGTCATTTGGAGCAG TTCGCGTTGGGTAAACTTCGAC	qPCR

Table S2, Refers to **Figure 3A**. **List of upregulated and downregulated genes in *pmt-2(RNAi)* and WT treated with tunicamycin compared to WT animals.** Excel Spreadsheet

Click here to Download Table S2

Table S3, Refers to **Figure 3B**. **List of upregulated genes from the four-way Venn diagram.** Excel Spreadsheet

Click here to Download Table S3

Table S4, Refers to **Figure 3C**. **Hierarchical clustering gene list.** Excel Spreadsheet

Click here to Download Table S4

Table S5, Refers to **Figure 4**. **Predominant GO terms of each cluster.** Excel Spreadsheet

Click here to Download Table S5

Table S6, Refers to **Figure 5**. **Phenotype from RNAi screen of autophagy genes.** Excel Spreadsheet

Click here to Download Table S6

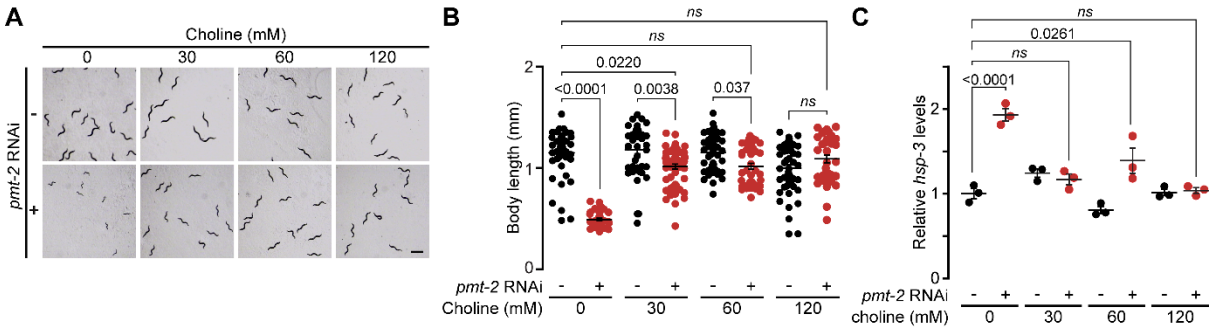

Figure S1, Refers to **Figure 1**. **Choline supplementation restores developmental defects in *pmt-2(RNAi)* animals.**
(A) Representative choline rescue assay of *pmt-2(RNAi)* developmental defect. L1 worms were grown on *pmt-2* RNAi or empty vector on plates supplemented with 0, 30, 60, or 120 mM choline, and images were taken after 48 h. Scale bar, 100 µm. (B) Body length quantification of worms from **A**. WT, 0 mM choline, n=47(-), n=32(+); 30 mM choline, n=39(-), n=58(+); 60 mM choline, n=48(-), n=43(+); 120 mM choline, n=54(-), n=38(+). (C) qPCR of *hsp-3* expression level in WT worms treated as in **A**. Data shown is the mean ± s.e.m. of at least three independent experiments. Statistical analysis was subjected to one-way ANOVA followed by Tukey's multiple comparisons adjustment. ns, non-significant.

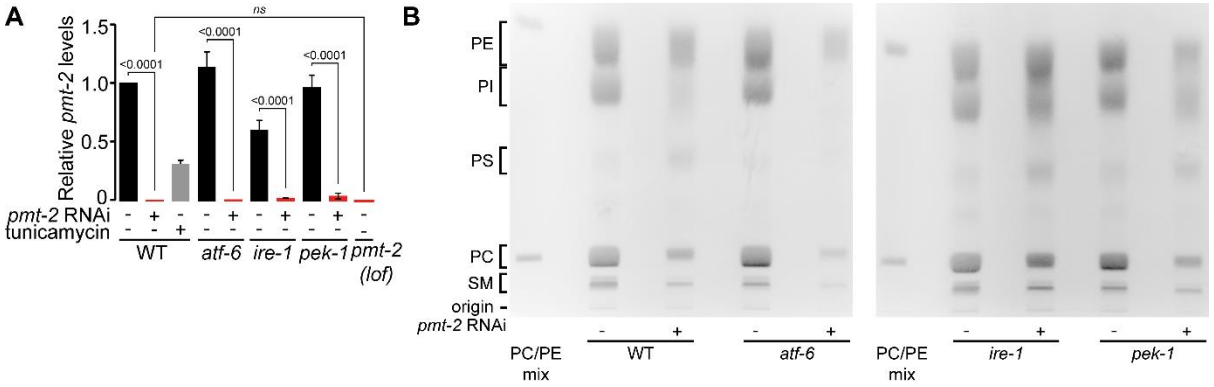

Figure S2, Refers to **Figure 2A-B**. **Inactivation of *pmt-2* decreased PC content in worms.**
(A) qPCR of *pmt-2* expression after *pmt-2* RNAi treatment in WT, *atf-6(lof)*, *ire-1(lof),* and *pek-1(lof)* worms. *pmt-2(lof)* worms were used as a control. *pmt-2* RNAi treatment efficiently silenced expression of *pmt-2* across all the strains tested. (B) Representative separation of PE, MMPE, DMPE, and PC from total lipid extract using thin-layer chromatography (TLC). Comparison of phospholipid levels in WT, *atf-6(lof)*, *ire-1(lof)* and *pek-1(lof)* animals treated with *pmt-2* RNAi. POPE (1-palmitoyl-2-oleoyl-sn-glycero-3-phosphoethanolamine; 16:0-18:1n9 PE) and DOPC (1,2-dioleoyl-sn-glycero-3-phosphocholine; 18:1n9 PC) were used as markers. Data shown is the mean ± s.e.m. of at least three independent experiments. Statistical analysis was subjected to one-way ANOVA followed by Tukey's multiple comparisons adjustment. ns, non-significant.

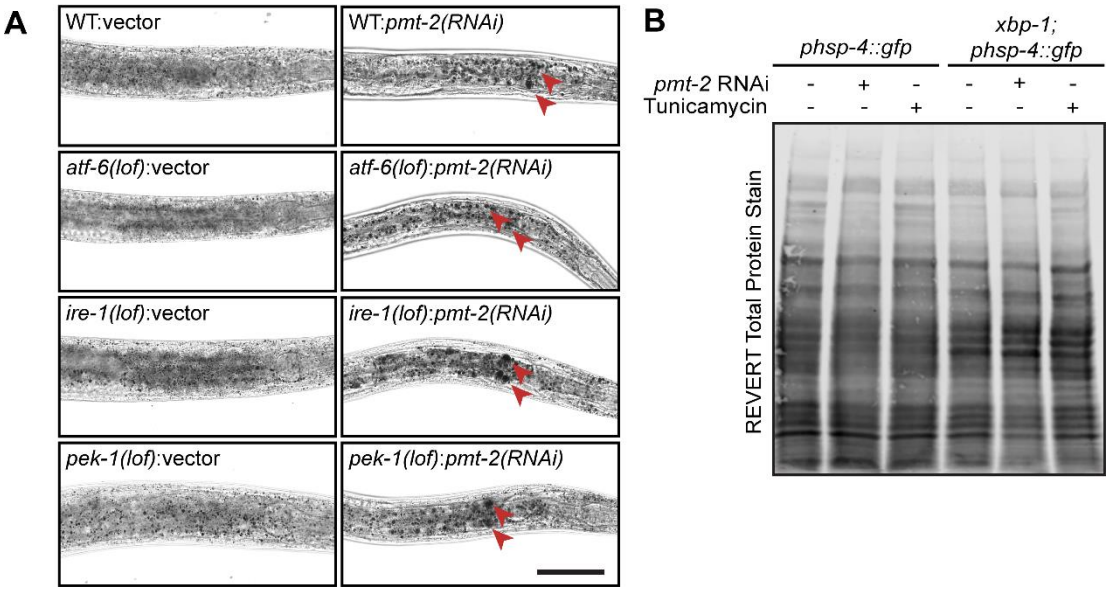

Figure S3, Refers to **Figure 2C,F**. **Lipid perturbation induces lipid droplets accumulation and activates the UPR.**
(A) Representative images of lipid droplet visualised using Sudan Black B staining of WT, *atf-6(lof)*, *ire-1(lof)* and *pek-1(lof)* animals treated with *pmt-2* RNAi. Brightfield images of stained worms are shown using 63X objective lens. Red arrowhead highlights large LDs. Scale bar, 100 µm. (B) Total protein stain verified equal loading and served as normalization control for the immunoblot.

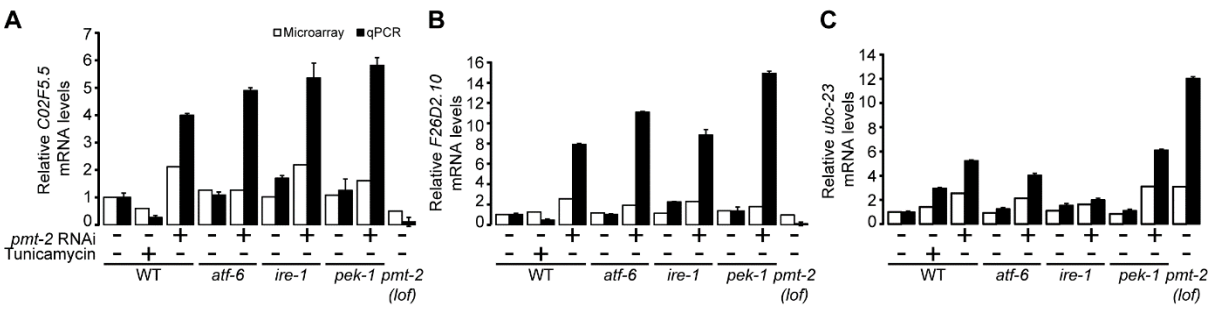

Figure S4, Refers to **Figure 3**. **Validation of DNA microarray analysis using quantitative real-time PCR.**
(A-C) Comparison of *C02F5.5* (A), *F26D2.10* (B), and *ubc-23* (C) gene expression in WT, *atf-6(lof)*, *ire-1(lof)* and *pek-1(lof)* animals treated with *pmt-2* RNAi by DNA microarray (white bars) and qPCR (black bars). *C02F5.5* and *F26D2.10*, are both uncharacterized genes; *ubc-23*, a member of the BCL-2 family. The figure represents technical triplicates.

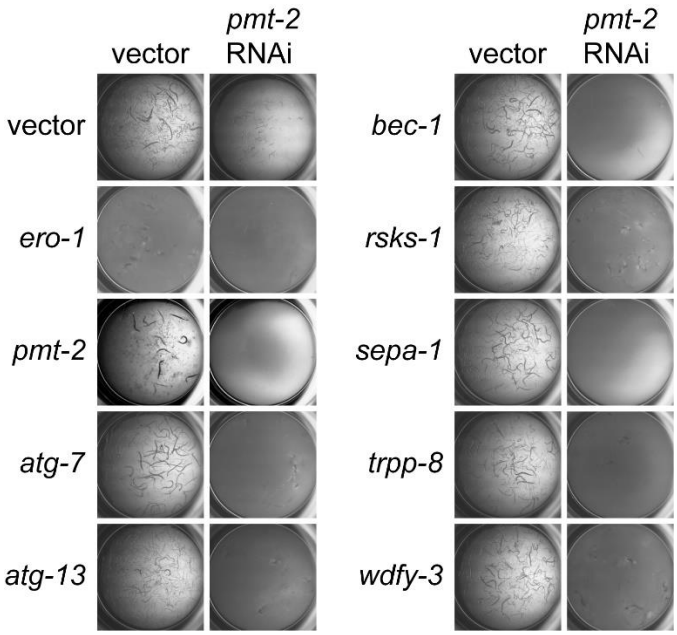

Figure S5, Refers to Figure 5. **Autophagy is essential during lipid perturbation.** WT worms were treated with vector or *pmt-2* RNAi for 36 h and subsequently subjected to RNAi in liquid media in a 96-well plate for 5 days. The worms were scored based on their developmental defects as described in Fig. 5A. *ero-1* RNAi was included as a positive control.

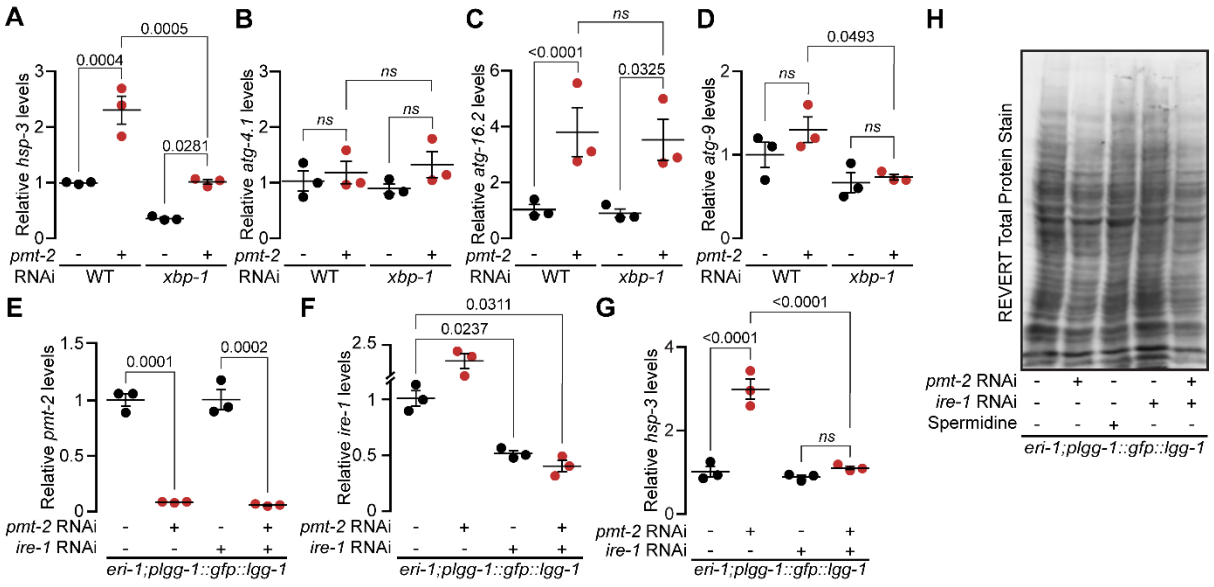

Figure S6, Refers to Figure 5. **Autophagy is partially dependent on XBP-1**. qPCR comparing expression of *hsp-3* (A), *atg-4.1* (B), *atg-16.2* (C), *atg-9* (D) in WT and *xbp-1(lof)* mutants treated with *pmt-2* RNAi. qPCR comparing expression of *pmt-2* (E), *ire-1* (F), *hsp-3* (G) in *eri-1;plgg-1::gfp::lgg-1* worms treated with *pmt-2, ire-1*, and *ire-1:pmt-2* RNAis; technical triplicates. (H) Total protein stain verified equal loading and served as normalization control for the immunoblot. Data shown is the mean ± s.e.m. of at least three independent experiments. Statistical analysis was subjected to one-way ANOVA followed by Tukey's multiple comparisons adjustment. ns, non-significant.

Table S1. Oligonucleotide primers used in the study.

Gene	Sequence (5' to 3')	Assay
act-1	AGGACTGGGTGCTCTTCTGG GAGCACGGTATCGTCACCAA	qPCR
atg-4.1	AGGAAGATGGAATCGAGGCAA TGCAACCCCATCCTTGATCC	qPCR
atg-9	ATGGAATCGTTCTTCTCACTG GCAGGAGGTATTGTATCTTCTC	qPCR
atg-16.2	ATGTGCTGGCTGGATCTTCG GAGCCGAATCTGATCTCGCAG	qPCR
atg-18	CCGAAGTCAGACACTAGTCGAG TCGGAACCGATTGGTTGCTTG	qPCR
bec-1	AAGCTCTGACTGGACATTCTCG GCGTCAGAGCAATCATTACAAAC	qPCR
atg-18	CCGAAGTCAGACACTAGTCGAG TCGGAACCGATTGGTTGCTTG	qPCR
C02F5.5	CATCTTTTGAGCTTATGATGGTGCT AAGCACCAAGGAACACGAGAT	qPCR
epg-4	CCAATTCCTCTTATCACACCA GTCGAAGAAGTAATCGAAACAG	qPCR
F26D2.10	CTCTTGTGGCAGCTCATGGT CGTGGATCAAAAACAGCGGC	qPCR
hsp-3	AGAAGGAGACCAAGTATGGAACC TGATACGGTTTCCTTGGTCGTT	qPCR
hsp-4	CATCTCGTGGAATCAACCCT TGACGTCAAGAAGGACAACA	qPCR
lgg-1	TCGTGATGGTCCTGGTAGAGT ACGCATCCAACTTCGTCCA	qPCR
ire-1	ACAATGGCTAGTCAGCGAGG CAATCCAGCCATCGGTTCCT	qPCR
pmt-2	AGAACGTGGTCATTTGGAGCAG TTCGCGTTGGGTAAACTTCGAC	qPCR

Table S2, Refers to **Figure 3A**. **List of upregulated and downregulated genes in *pmt-2(RNAi)* and WT treated with tunicamycin compared to WT animals.** Excel Spreadsheet

Click here to Download Table S2

Table S3, Refers to **Figure 3B**. **List of upregulated genes from the four-way Venn diagram.** Excel Spreadsheet

Click here to Download Table S3

Table S4, Refers to **Figure 3C**. **Hierarchical clustering gene list.** Excel Spreadsheet

Click here to Download Table S4

Table S5, Refers to **Figure 4**. **Predominant GO terms of each cluster.** Excel Spreadsheet

Click here to Download Table S5

Table S6, Refers to **Figure 5**. **Phenotype from RNAi screen of autophagy genes.** Excel Spreadsheet

Click here to Download Table S6